DESIGN AND ASSESSMENT OF AN INNOVATIVE THERMAL MANAGEMENT SYSTEM FOR ELECTRONIC COOLING USING PCMS

by

Yahya Abdulrahman Sheikh Mohammed

A Thesis presented to the Faculty of the
American University of Sharjah
College of Engineering
In Partial Fulfillment
of the Requirements
for the Degree of

Master of Science in
Mechanical Engineering

Sharjah, United Arab Emirates

July 2020

Declaration of Authorship

I declare that this thesis is my own work and, to the best of my knowledge and belief, it does not contain material published or written by a third party, except where permission has been obtained and/or appropriately cited through full and accurate referencing.

Signed……Yahya…….

Date……23/7/2020……

Approval Signatures

We, the undersigned, approve the Master's Thesis of Yahya Abdulrahman Sheikh Mohammed.

Thesis Title: Design and Assessment of an Innovative Thermal Management System for Electronic Cooling Using PCMs.

Date of Defense: 16/7/2020

Name, Title and Affiliation	**Signature**
Dr. Mohamed Gadalla Professor, Department of Mechanical Engineering Thesis Advisor	
Dr. Mohammad Nazzal Associate Professor, Department of Mechanical Engineering Thesis Committee Member	
Dr. Zarook Shareefdeen Professor, Department of Chemical Engineering Thesis Committee Member	
Dr. Mamoun Abdel-Hafez Head Department of Mechanical Engineering	
Dr. Lotfi Romdhane Associate Dean for Graduate Studies and Research College of Engineering	
Dr. Sirin Tekinay Dean College of Engineering	
Dr. Mohamed El-Tarhuni Vice Provost for Graduate Studies Office of Graduate Studies	

Acknowledgement

I would like to thank my advisor Dr. Mohamed Gadalla for providing guidance, and support throughout my research stages. I am deeply beholden for his assistance, suggestions.

I express my deepest gratitude to my late advisor, Dr. Saad Ahmed (may Allah have mercy on him), for accepting me to be his student, and for his kindness.

In addition, I would like to thank the professors of the college of engineering who taught me the master level courses with mighty teaching methods and skills.

My gratitude to American University of Sharjah for providing me with Graduate Teaching Assistantship (GTA) fund that helped me financially and allowed me to gain useful teaching and work experience.

Abstract

Thermal management of electronics is an important issue since the reliability of electronic components is greatly affected by the operating temperature. Electronics, such as laptops, are becoming more likely to overheat as their dimensions become smaller. Overheating an electronic device can cause problems such as a sudden shutdown, system freezing, and most importantly, it will affect its lifetime. To overcome this problem, a small vapor compression refrigeration (VCR) system integrated with Phase change materials (PCMs) is proposed. PCMs could be effective when electronic cooling systems such as heat sinks are considered. However, bio-based PCMs have poor thermal conductivity and therefore suffer from poor heat transfer characteristics. The diffusion of certain additives within the PCM has proven successful in the enhancement of heat transfer during the cooling process. Graphene Nanoplatelets (GNPs) presents itself as one such additive. This work experimentally investigates the cooling performance of the heat sink when GnPs and Graphite with various surfactants such as Sodium Dodecyl Sulfate (SDS), Sodium Dodecylbenzene Sulfonate (SDBS) and Sodium Stearoyl Lactylate (SSL) are added to the bio-based PCM. SSL NanoPCM provided a 345-sec delay compared to the Pure PCM, and the response time of PCM was improved be 51% when it was mixed with GnPs at 5% mass fraction. SDS surfactant indicated the highest increase in thermal conductivity when compared to others as it reported the highest increase of 368% when compared with the thermal conductivity of PurePCM. The main objective of this work is to design a new active cooling system to cope with increasing demand for powerful and high-performance electronics. The system is made of a compressor, an expansion device, a condenser, an evaporator, a fan, and a cold storage. The system is designed for laptop cooling with a cooling capacity of 100W and the dimension of the system is 38 × 30 × 15 cm. A comprehensive thermodynamic analysis was performed. While modelling the performance of the system, it is found that R134a has the best performance among the others. When the laptop cooler was used, the maximum temperature of the central processing unit (CPU) was found to be 67 °C, while it was 78 °C without using the cooler. Noticeably, using the cooler helped in reducing the temperature of CPU by 11 degrees (14.1%).

Keywords: ***Electronic Cooling; PCM; Miniature Vapor Compression System; Graphene Nanoplatelets; Graphite; Surfactants.***

Table of Contents

List of Figures

List of Tables

List of Symbols and Abbreviations

Symbols

A_s	Heat transfer surface area (m^2)
b	Coefficient of volume expansion (1/K)
C_p	Specific heat (kJ/kg.K)
g	Gravitational acceleration (m/s2)
h	The average heat transfer coefficient. (w/ m^2.k)
h_1	Specific enthalpy at the evaporator outlet *(*J/g)
h_2	Specific enthalpy at the condenser inlet (J/g)
h_3	Specific enthalpy at the condenser outlet (J/g)
h_4	Specific enthalpy at the evaporator inlet (J/g)
K	Thermal conductivity (w/m. K)
L	Specific latent heat of the PCM (J/g).
Lc	Characteristic length of the geometry (m)
m	Mass (kg)
m_{PCM}	The mass of PCM (g).
$\dot{m}_{ref}$	The mass flow rate of the refrigerant (g/s)
n	Kinematic viscosity of the fluid (m^2/s)
$\dot{Q}_e$	Heat rate taken by the evaporator (W).
$\dot{Q}_c$	Rejected heat rate by condenser (W).
T∞	Temperature of the surrounding air (°C)
Ts	Temperature of the surface (°C)

Abbreviations

CPU	Central Processing Unit
GnPs	Graphene Nanoplatelets
PCM	Phase change material
PCMs	Phase change materials
SDBS	Sodium Dodecylbenzene Sulfonate
SDS	Sodium Dodecyl Sulfate
SSL	Sodium Stearoyl Lactylate
VCR	Vapor Compression Refrigeration

Chapter 1. Introduction

In this chapter, we provide a short introduction about the thermal management of electronics and the encountered problems in this area. Then, we present the problem investigated in this study as well as the thesis contribution.

1.1. Overview

Thermal management of electronics is an important issue since the reliability of electronic components is greatly affected by the operating temperature. A drop in performance, failure of critical components and user discomfort are the result of improper thermal management. Nowadays, the physical dimensions of electronics are becoming smaller as well as the space available for thermal management, so cooling electronics has become a big challenge [1].

According to U.S. Air Force survey , more than 50% of the total electronics failures are temperature-related Failures [2]. Overheating of electronics or even a small difference in operating temperature of electronics can cause a reduction in the lifetime of electronics or a failure [3]. Therefore, Thermal management has become a critical factor in the design of electronics to maintain the temperature in a certain range, preventing electronic components from failure. The change in electronics temperature is a result of heat generated from high-power-density integrated circuits or changes in the ambient temperature [4]. The operating temperature range of Conventional electronic components is 0 °C to 70°C.

1.2. Thesis Objectives

The main objectives of this work are to design a new active cooling method that is needed to cope with increasing demand for powerful and high-performance electronics, to find the best candidate as a cold storage medium for electronic cooling with its additives, and to evaluate the selected materials based on their Cooling performance.

1.3. Significance of Research

The contributions of this research work can be summarized as follows:

- Propose an innovative way of electronics cooling that can protect the electronics against overheating.

- Propose an innovative thermal management system that can remove heat from electronics operating in indoor, outdoor and other types of environments.

Chapter 2. Background and Literature Review

2.1. Types of Thermal Management Systems

Managing heat, which is generated by electronics, is a critical factor in electronics' design to improve their reliability and performance and to prevent failure. Efficient thermal management can maintain the temperature of electronics within the operating range to cope with the demand for smaller and powerful electronics. Several techniques of thermal management for electronic cooling are shown below.

2.1.1. Air cooling. Air cooling, the simplest technique of thermal management for electronic cooling, can be operated as both active and passive. When natural convection is insufficient to remove heat, Forced air cooling, which uses fans, is used to increase heat transfer from the electronics to the ambient air [5].

2.1.2. Heat sinks. A material with high thermal conductivity such as aluminium is used to make Heat sinks. Heat sinks that are sometimes used in combination with a fan transfer the heat generated by an electronic to the surrounding air.

2.1.3. Liquid cooling. Liquid Cooling is a highly effective method of removing heat compared to Air Cooling, because of its high specific heat capacity and thermal conductivity. The electronic components are in direct contact with the liquid; therefore, the liquid absorbs the heat generated by electronics and transfers the heat to the ambient air. Liquid Cooling could be both active and passive. It is better to use active liquid cooling when the temperature difference between the electronic device and the surrounding air is small [5].

2.1.4. Heat pipes. A heat pipe, which a hollow tube containing a liquid, is commonly preferred thermal management solution for electronics it uses evaporation and condensation of a liquid to absorb the heat from electronic components. Because of its high efficiency, a heat pipe is used to cool down many desktop CPUs. Figure 2.1 shows the structure of a heat pipe.

2.1.5. Thermoelectric cooling. The thermoelectric module is a way to remove thermal energy from electronics by creating a temperature difference when the electric voltage is applied across joined conductors. It transfers heat from one side to the other side. The thermoelectric module is used to pump heat away from the electronic devices. It can provide precise temperature control. However, there is a drawback to

thermoelectric cooling related to its efficiency. It is generally around 40% as efficient as a conventional compression cycle system; however, a thermoelectric cooling may be more practical and cost-effective than a conventional refrigeration system on a small scale. The thermoelectric architecture for cooling electronic equipment is shown in Figure 2.2.

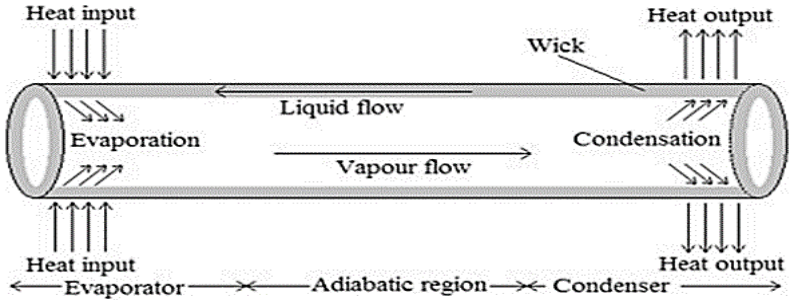

Figure 2.1: The structure of a heat pipe [6].

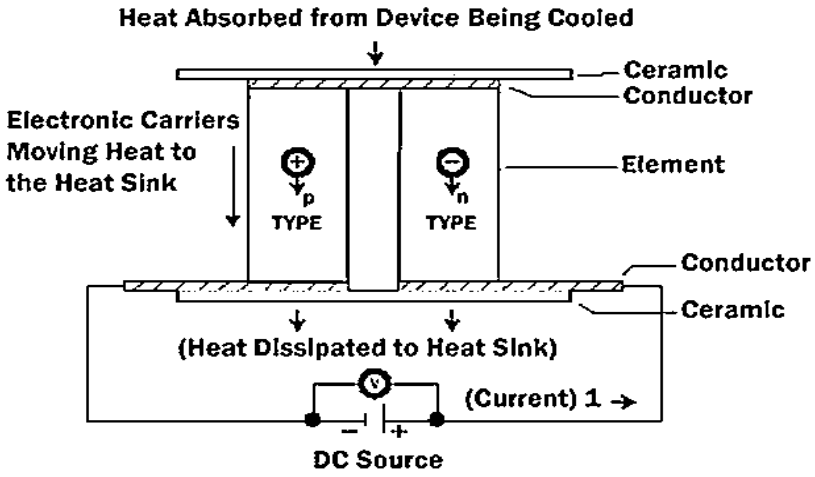

Figure 2.2: Schematic of thermoelectric [7].

2.1.6. Vapor compression system. The vapor-compression, which uses a circulating refrigerant as the medium, is an extremely effective way to cool electronics. The refrigerant absorbs and removes heat from the electronics to the surrounding air. The compressor, condenser, expansion valve, and evaporator are the major elements of a refrigeration system. Figure 2.3 shows a schematic representation of the vapor compression cycle.

2.1.7. Phase change materials. Phase Change Materials, which can store a large quantity of heat due to their heat of fusion, are considered as the best solution for thermal management. Phase Change Materials, which are classified as latent heat storage units, can store and release heat at an almost constant temperature when they

undergo a phase change from solid state to liquid state or vice versa. Phase Change Material has attracted increasing interest from researchers due to its lightness, compactness and high latent heat of fusion.

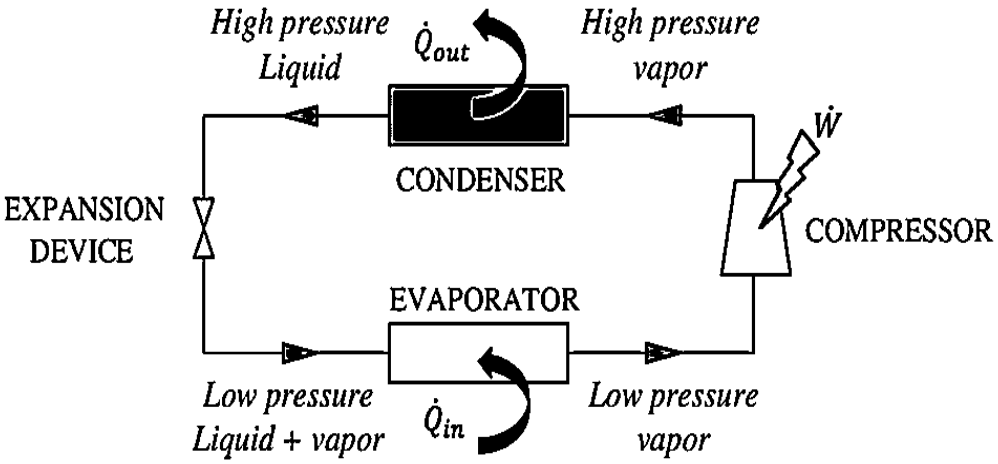

Figure 2.3: Vapor compression cycle [8].

2.2. Advantages and Disadvantages of Thermal Management Systems

Siddique et al. [9] reviewed comprehensively some of Thermal management systems as shown in Table 2.1.

2.3. Types of PCMs

Thermal energy storage, which involves the storage of heat in one of two forms; Sensible heat and Latent heat can be used for electronics cooling. Compared to conventional sensible heat energy storage, for the same amount of energy that is needed to be stored, a latent heat storage system requires lower weights and fewer volume changes of material [10].

By utilizing the latent heat of fusion during the process of melting or freezing, Phase change materials (PCMs) absorb and release thermal energy. Nowadays, there are more than five hundred Types of PCMs available, but only a few of them have the properties that could be used for thermal management. The two most important requirements are having a suitable phase change temperature and having a large melting enthalpy. The typical range of melting enthalpy and melting temperature of common material classes used as PCM is shown in Figure 2.4. Water is the best-known PCM. It has been used for cold storage for more than 2000 years. Several material classes cover the temperature range from 0 °C to about 130 °C [11].

Table 2.1: Advantages and disadvantages of TMSs.

Thermal management systems	Types	Advantages	Disadvantages
Passive system	Air cooling	✓ Low initial cost ✓ Easy maintenance	⅄ Low specific heat ⅄ Low efficiency
	Liquid cooling	✓ Low initial cost ✓ Easy and low maintenance cost	⅄ Leakage possibility
	Heat pipe	✓ High thermal conductivity ✓ High efficiency	⅄ Expensive ⅄ Leakage problem
	PCM	✓ Low cost ✓ Reliable and long lasting operation ✓ Higher efficiency	⅄ Low thermal conductivity ⅄ Leakage problem
Active system	Forced air (using fan)	✓ Direct contact ✓ Light weight	⅄ Low specific heat ⅄ Costly
	Liquid cooling (using al pump)	✓ Higher heat capacity ✓ High efficiency	⅄ Expensive ⅄ Leakage problem
	Thermoelectric cooler	✓ Static device ✓ longer operational lifetime	⅄ Low efficiency ⅄ Additional power requirement

2.3.1. Organic PCMs. Organic PCMs are subdivided into paraffin and bio-based PCMs.

2.3.1.1. Paraffins. Paraffins are derived from petroleum. Their melt point temperatures range between -8°C and 40°C. They are non-corrosive and are compatible with most encapsulation materials. However, they have a limited range of melting points and their cost is linked to unstable petroleum prices.

2.3.1.2. Bio-based PCMs. They derived from animal fat and plant oils, were investigated as PCMs in TES systems because of their suitable phase change temperature, high latent heat density, low cost, ready availability, non-toxicity, and non-flammability [12]. Their melt point temperatures range between -40°C and 151°C.

2.3.2. Inorganic PCMs. They can be divided into hydrated salts and metallic.

2.3.2.1. Salt hydrates. They consist of salts and water. Their melt point temperatures range between 15°C and 80°C. The advantages of salt hydrates are low material costs, high latent heat storage capacity, and high thermal conductivity. The main problems with salt hydrates are their lower thermal stability. Following each cycle, some salt hydrates fail to entirely recrystallize. Eventually, they lose all latent heat capacity.

2.3.3. Clathrate hydrates. Most hydrates, which are ice-like crystals, can be formed at a temperature above the freezing point of water under different pressures. The refrigerants gas hydrates, which almost have the same fusion heat of ice, can be considered as promising energy storage materials, especially for air conditioning systems [13]. Most refrigerant hydrates can be formed under low pressure (below one MPa) with suitable phase change temperature for air-conditioning and large fusion heat (270–430 kJ/ kg) [14]. Clathrate hydrates cover a temperature range from about 0 °C to 30 °C. PCMs are sub-grouped as organic and inorganic. A brief detail of PCMs' classification is shown in Figure 2.4.

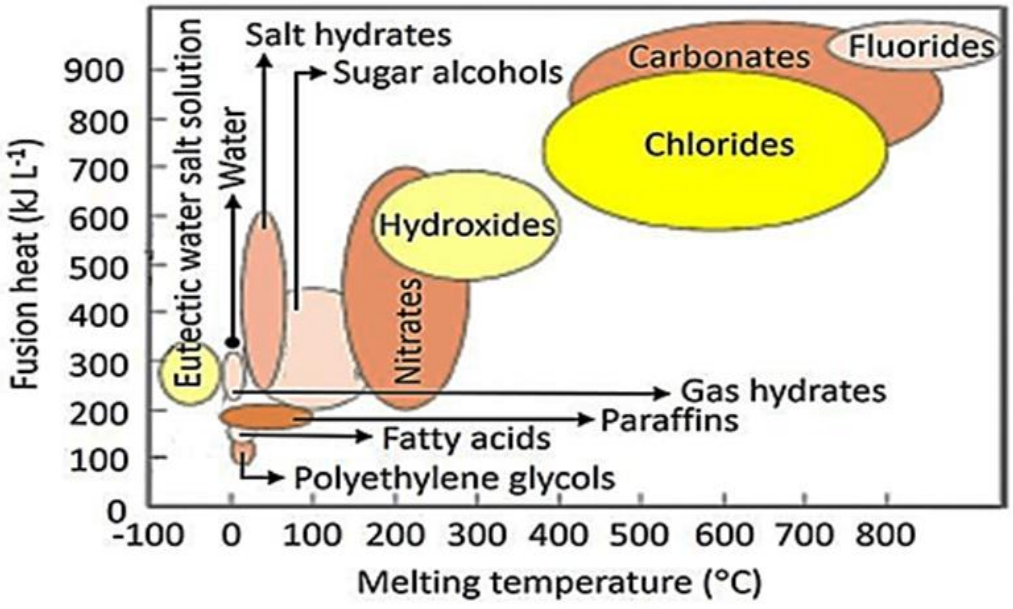

Figure 2.4: Melting temperature and fusion heat of different PCMs [11].

2.4. Numerical and Experimental Study Related to Electronics Cooling Using PMCs

In the last few years, a new direction of Thermal Management of electronics using Phase Change Materials (PCMs) has been introduced. Researchers used different PCM based passive techniques for electronic cooling. PCM absorbs and stores heat while the electronic device is operating. When the electronic device is idle, the melted PCM disperses heat to the surroundings and re-solidifies. There are many researches about PCMs for the thermal management of electronics.

Alawadhi and Amon [15] presented a thermal management system using eicosane as the PCM with the phase change temperature of 37 °C to cool a portable device. Different heating rates, heating periods, and the number of fins were examined. They concluded that using PCM could provide a reliable solution to portable electronic devices to avoid overheating and thermally-induced fatigue.

Hassan et al**.** [16] investigated and compared the performance of three different types of PCMs namely salt hydrate, paraffin wax, and milk fat in PCM based finned heat sink system under natural and forced convection at different heat loads. It was found that using PCM could extend the time for the electronic device to operate under safety temperature to 5 minutes under natural convection and 15 minutes under forced convection or the same heat load.

Kandasamy et al. [17] investigated the use of PCM-based thermal management system in mobile devices for power levels ranging from 6 to 12 W and the performance of the system under different orientations of the package to gravity. They used paraffin wax in their research with a heat sink having a minimum thickness of 10 mm. It is found that a PCM is a practical thermal solution at a higher heat power.

2.4.1. Literature work. In the last few years, Different PCMs have been used for electronic cooling. Table 2.2 shows the summary of the literature work done.

2.5. Numerical and Experimental Study Related to Electronics Cooling Using Mini Refrigeration System (Refrigerated Heat Sink).

The miniature vapour compression refrigeration system is one of the most promising cooling techniques for electronics cooling in general and high heat dissipation electronics cooling in particular. The evaporator of the refrigerated heat sink is mounted directly to the chip. It maintains the operating temperature of electronics below the ambient air temperature, increases the reliability of electronics.

Table 2.2: Summary of the literature work review.

Author	The work	PCM
Alawadhi and Amon [15]	investigated numerically and experimentally the performance of using PCM for electronics cooling.	Petroleum-based
Hassan et al.[16]	investigated the performance of different PCMs that were integrated within the heat sink.	Salt hydrate, Petroleum-based and Bio -based
Kandasamy et al.[17]	investigated experimentally the feasibility of using PCM for transient electronic cooling.	Petroleum-based
Tomizawa et al.[18]	Investigated numerically and experimentally the effectiveness of using PCM sheets for mobile phones.	Petroleum-based
Tousif et al.[19]	Investigated experimentally the performance of using two different PCMs for Tablet PCs cooling.	Bio-based and Petroleum-based
Tan and Tso[20]	conducted experimental study of electronics cooling using PCM.	Petroleum-based
Hosseinizadeh et al.[21]	Investigated numerically and experimentally the application of a PCM-based heat sink for cooling computer chip.	Petroleum-based
Sahoo et al.[22]	Investigated experimentally the performance of a fan (PCM)-based cooling system.	Petroleum-based
Motahar and Khodabandeh [23]	Investigated experimentally the thermal performance of a Nano-PCM-based heat sink.	Petroleum-based

Over the past decade, extensive experimental and analytical studies of using the miniature compression refrigeration system for electronics cooling has been conducted.

Mongia et al. [24] built a miniature refrigeration system with COP higher than 2.25 for the cooling notebook using a high-efficiency compressor . The system with isobutene (R600a) as the working fluid achieved a cooling capacity of 50 W.

Nnanna [25] designed and built a VC Refrigeration System for electronics cooling to study the transient response of the refrigeration system operating with R134a to variation of applied loads. Compared to the conventional air-cooling system, the VC Refrigeration system maintained the junction temperature of the simulated electronics at a much lower temperature.

Trutassanawin et al. [26] designed and fabricated a miniature refrigeration system, using R-134a as the refrigerant, to investigate the feasibility of using it in electronics cooling. The compressor design cooling capacity varies from75–140 W and a COP of 1.13–1.35. The compressor failed after 50 steady-state performance tests because the compressor was not designed for the operating conditions of electronics cooling.

Chang et al. [27] experimentally investigated the thermal performance of a miniature R-134a refrigeration for electronic cooling. The system achieved the largest cooling capacity of 150 W with a COP of 4.25.

Mancin et al. [28] designed and tested a miniature R134a compression refrigeration system using an oil-free linear compressor for electronic cooling with cooling capacity varied from 37 W to 374 W. The COP ranged from 1.05 to 5.80 accordingly.

Wu and Du [29] designed, built, and tested a miniature R134a compression refrigeration system for electronics cooling with a cooling capacity of 200 W. The COP ranged from 5.7 to 8.6 and the efficiency of the system varies from 23% to 31%. Figure 2.5 shows a schematic representation of the miniature VCR system.

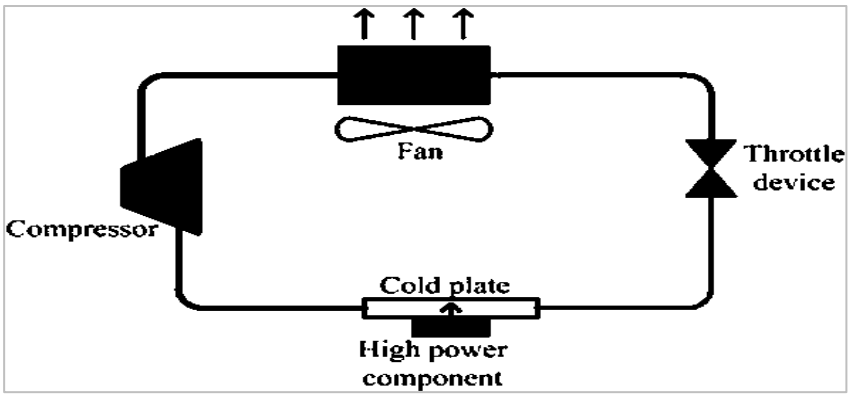

Figure 2.5: Schematic of the miniature VCR system [29]

To the best of our knowledge, no study has been carried out investigating the performance of using refrigerated PCM heat sink for electronics cooling. A Small

Vapor Compression Refrigeration (VCR) system integrated with PCM is proposed to cope with the increasing demand for smaller and powerful electronics.

2.6. Study Related to Enhancing The Thermal Conductivity of Bio-based PCM Using Graphene Nanoplatelets (GNPs)

Most PCMs have very low thermal conductivity, so they take time to charge and discharge, which limits their practical applications. So, using Additives is required to improve the thermal conductivity, therefore it will reduce the charging or discharging time of PCMs.

In the last few years, many studies used GNPs to enhance the thermal conductivity of Organic PCM whether it is Bio-based PCM or Petroleum-based PCM. Table 2.3 shows the summary of the literature work done

Table 2.3: Summary of the literature work review

Author	The work	PCM	thermal conductivity enhancement %
Parlak et al. [30]	investigated experimentally the thermal performance and energy storage capabilities of PCM	Petroleum-based	300 %
Mehrali et al.[31]	investigated experimentally the effect of graphene addition on the thermal conductivity of PCM	Bio-based	630 %
Temel et al.[32]	examined heating performances of GNP/PCM composites in an energy storage unit	Petroleum-based	253 %

Parlak et al. [30] evaluated the thermal performance of petroleum-based PCM / (GNPs) composites at various mass fractions. They found that the thermal conductivity of PCM increased by 300 % when it is mixed with GNP at 10% mass fractions.

Mehrali et al. [31] investigated experimentally the effect of graphene (GNPs) addition on the thermal conductivity of PCM. GNPs absorbed a maximum of 91.94 wt% of Bio-based PCM via a vacuum impregnation method. They found that thermal conductivity of PCM increased by about 630 %.

Temel et al. [32] evaluated heating performances of petroleum-based PCM / (GNPs) composites at various mass fractions. They found that the thermal conductivity of PCM increased by 253 % when it is mixed with GNP at 7% mass fractions

To the best of our knowledge, no study has been carried out using GnPs to enhance the thermal conductivity of bio-based PCM produced by the PureTemp. PureTemp PCM has low flammability and is biodegradable. It has high latent heat and a range of different melting points, making it ideal for use in textiles, HVAC, and applications requiring thermal management above room temperature.

This work investigates experimentally the effects of adding GnPs with different mass fractions to PureTemp PCM and using it as a heat sink to absorb the heat away from a high temperature object (a heater).

2.7. Study Related to Enhancing the Thermal Conductivity of Bio-based PCM Using Graphite

Recently, there has been growing research into the study of improving the thermal conductivity of PCMs. The use of conductive-additives has been one of the more recent techniques that have been used in order to augment the thermal conductivity of the PCM. In this technique, conductive-additives diffused within the PCM, forming a PCM composite, which would exhibit decreased charging and discharging time of the PCM. There are numerous such additives to select from and there exist a large variety of methodologies that can be employed when forming the mixture.

Many researchers have attempted to increase the thermal conductivity of PCM through the addition of expanded graphite or similar graphite nanoparticles. Ling et al. [33] utilized expanded graphite (EG) particles to improve the thermal conductivity of RT44HC, which is an organic PCM. Results indicated that the two main impacting factors for improving thermal conductivity are bulk density of the composite mixture and mass fraction of EG. Increases in these two properties led to a substantial increase in the thermal conductivity of the mixture up to 60 times. Wang et al. [34] dispersed graphite nanoparticles into a paraffin/water emulsion to improve thermal conductivity.

The study illustrated a 20% improvement in thermal conductivity relative to pure paraffin emulsion with a 0.1 wt% Graphite. Xu et al. [35] tested the enhancement of thermal management through increasing thermal conductivity by using a D-Mannitol/EG composite. The results showed an increase in thermal conductivity by 12 times for 15-wt% EG.

Even though it improves thermal conductivity, the addition of graphite nanoparticles into organic PCMs results in poor stability and reduced thermal performance due to aggregation and sedimentation [36, 37]. To neutralize this effect, studies suggested the addition of chemical substances called surfactants. Surfactants are composed of amphipathic molecules that utilize electrostatic stabilization through adjusting the surface charge of the nanoparticles causing appropriate dispersion of these additives in organic PCMs [37]. Zhang et al. [36] added multiwall carbon Nano-tube (MWCNT) particles to n-hexadecane to reduce supercooling but an aggregation of the MWCNT particles reduced its effectiveness. However, through the addition of strong acids H2SO4 and HNO3 as well as 1-decanol of surfactant to the MWCNT particles, the mixture was able to reduce supercooling through effective dispersion of the MWCNT particles. Choi et al. [38] investigated the effect of carbon additives on the thermal conductivity of PCM and used Poly Vinyl Pyrrolidone (PVP) as a surfactant to enhance dispersion stability; as a result, aggregation is reduced and the thermal management capabilities of the system are improved. Figure 2.6 shows the Preparation of surfactant-coated particles.

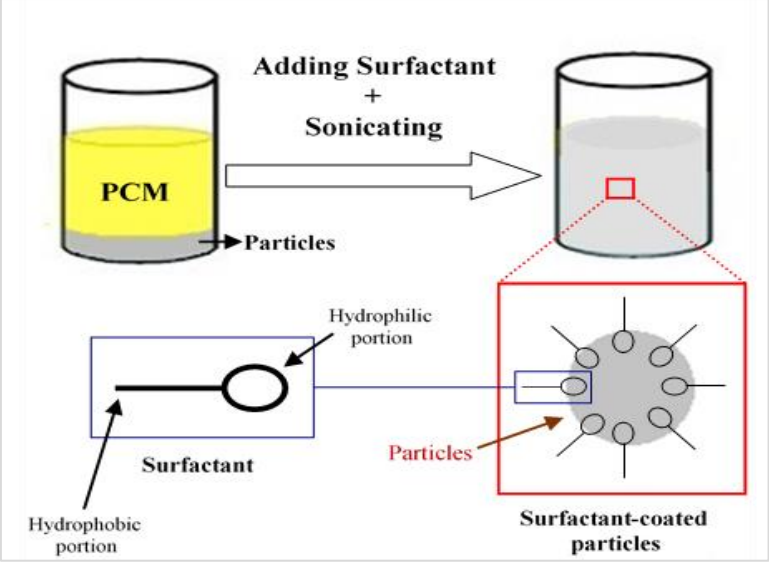

Figure 2.6: Preparation of surfactant coated particles

Chapter 3. Research Methodology

In this chapter, we formulate the problem of shortages in active cooling techniques for electronics and how can we tackle them appropriately. We also present the proposed thermal management systems for laptop cooling.

3.1. Problem Formulation

Managing heat, which is generated by electronics, is a critical factor in electronics' design to improve their reliability and performance and to prevent failure. Efficient thermal management can maintain the temperature of electronics within the operating range. Conventional cooling techniques that are aimed at rapidly removing the heat from the electronics to the surrounding air become incompetent, as their cooling capability is limited. Therefore, new active cooling methods are needed to cope with the demand for powerful and high-performance electronics.

Since the dimensions of electronics such as laptops are becoming smaller, they are becoming more likely to overheat. Overheating does not only reduces the life expectancy but it also leads to product failure. The change in electronics temperature is a result of heat generated from high-power-density integrated circuits or changes in the ambient temperature.

3.2. System Model

To overcome these two problems, we proposed an innovative thermal management system for electronics cooling PCM as a storage medium. A small refrigeration system is used as a laptop cooler.

The proposed system that consists of a compressor, evaporator, condenser, and expansion valve has the ability to cool the electronics below the surrounding temperature. A fan is used to generate additional airflow around the body of the laptop. Figure 3.1 shows a schematic diagram of the proposed system during charging the encapsulated PCM (indirect cooling and indirect-contact heat transfer.

3.3. Working Principle of the Design

First, the pressure of a vapour refrigerant is increased, when it travels through the compressor. Then the refrigerant starts to condense when it passes through a condenser, by transferring heat to the surrounding air. Next, the refrigerant passes

through an expansion device, which reduces the pressure of the liquid refrigerant, and when the low-pressure liquid refrigerant enters the evaporator, it begins to evaporate and absorbs the heat from its surrounding due to the fact that the lower the pressure the lower the temperature at which the phase change will happen. Lastly, the vaporized refrigerant re-enters the compressor and the process is repeated. The evaporator is attached to the PCM container (Cold Storage) so that the heat from the container is transferred to the evaporating refrigerant.

During the charging process, the PCM starts to solidify by giving out the heat into evaporator. The process will last until the PCM becomes solid, then the compressor will be shut down.

In order to cool the surrounding air, it is forced into contact with the PCM using a fan, as a result, heat exchange occurs and the air is cooled. During this process, called discharging, the heat is transferred from the air to the PCM. During the phase change, a large amount of heat will be absorbed by the PCM without changing its temperature. The discharging process will last until the PCM becomes liquid. Figure 3.2 shows a schematic diagram of the proposed cooling system.

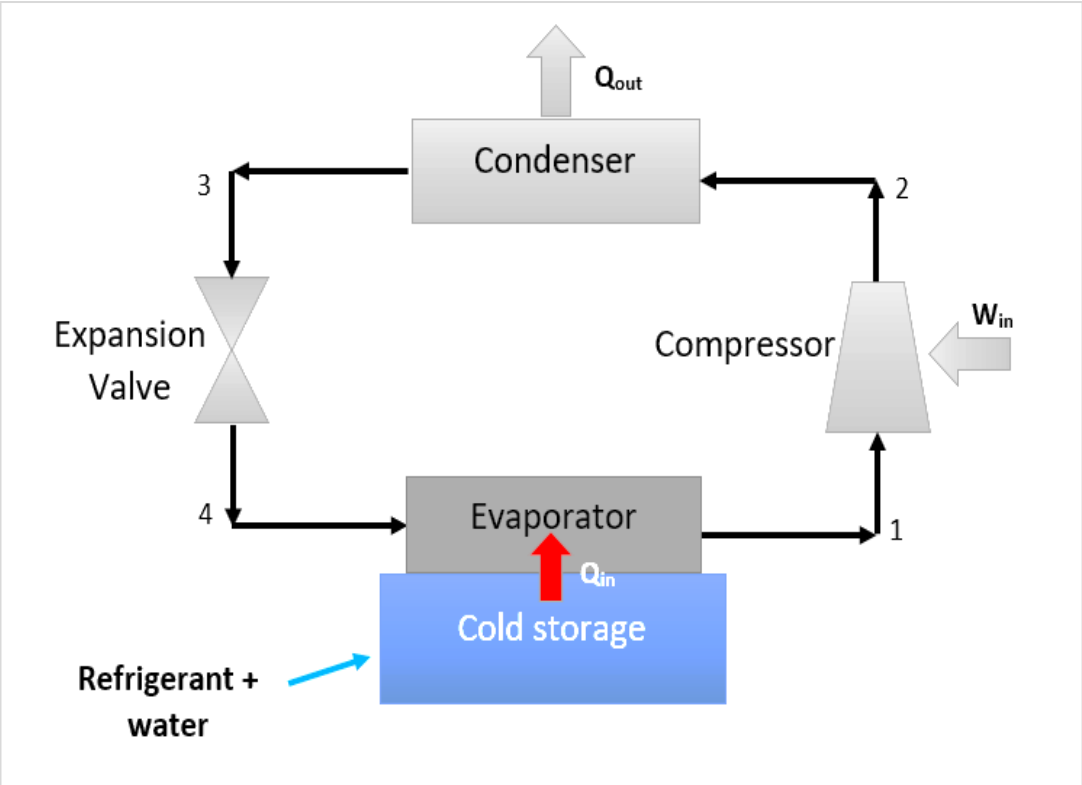

Figure 3.1: Schematic diagram of the proposed system during charging the PCM (indirect cooling and indirect-contact heat transfer)

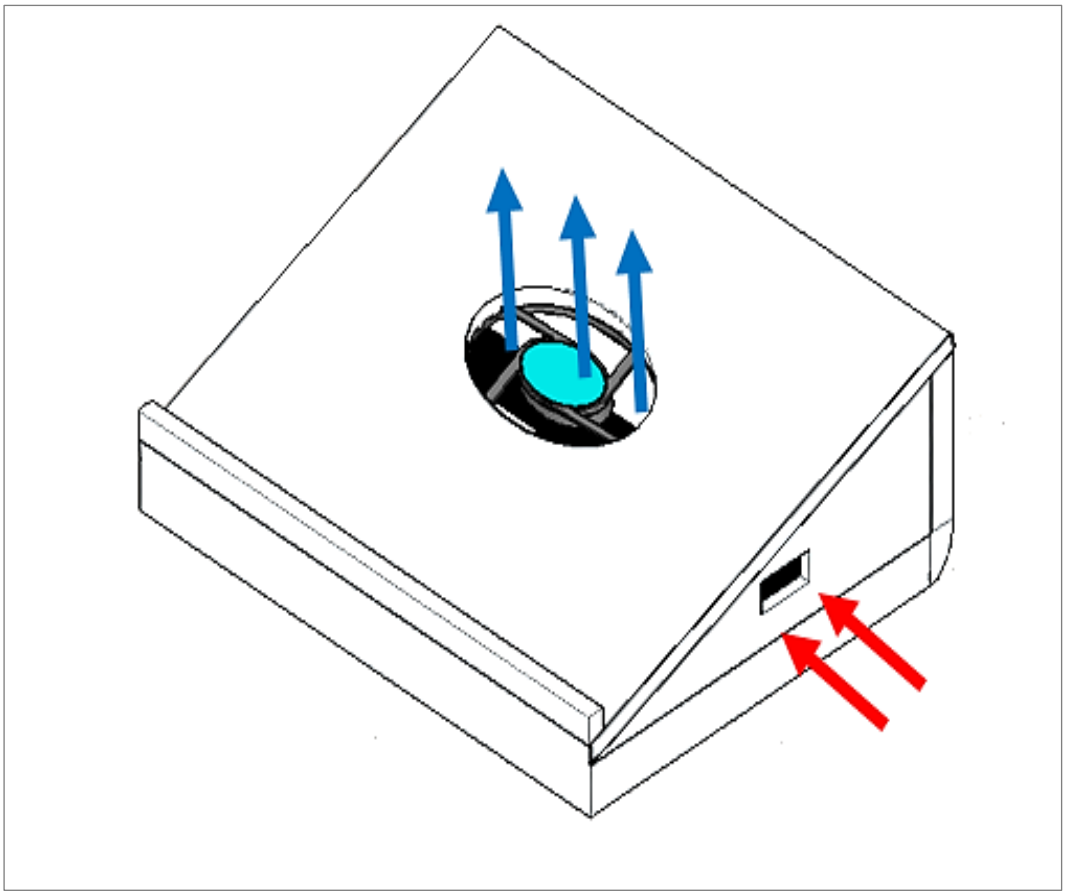

Figure 3.2: Schematic diagram of the proposed cooling system (indirect cooling).

3.4. Material Selections

3.4.1. Compressor. Acompressor is a critical component of the vapour-compression refrigeration system. Aspen's compressor, rotary-type with a 6.7 cm diameter and 8.8 cm height, is the best choice since it is the smallest device available on the market, can operate with different refrigerants (R134a / R404a / R410a /R290a / R600a), Its noise level is about 40 dB and it weighs about 1 kg.

3.4.2. Condenser, Cold storage, evaporator and finned plate. The condenser is heat exchanger model with a size of 20 × 10 × 2 cm. The dimensions of Cold storage, evaporator, and a finned plate will be 34 × 4 × 2 cm, 32 × 3 × 2 cm and 34 × 4 × 2 cm, respectively.

3.4.3. Throttling device. The capillary tube is used as the throttling device since it has no moving parts and is easier and cheaper to replace. The inner diameter of the capillary tube is 0.8 mm with a length of 1800 mm.

Figure 3.3 shows the suggested design for the laptop-cooling stand.

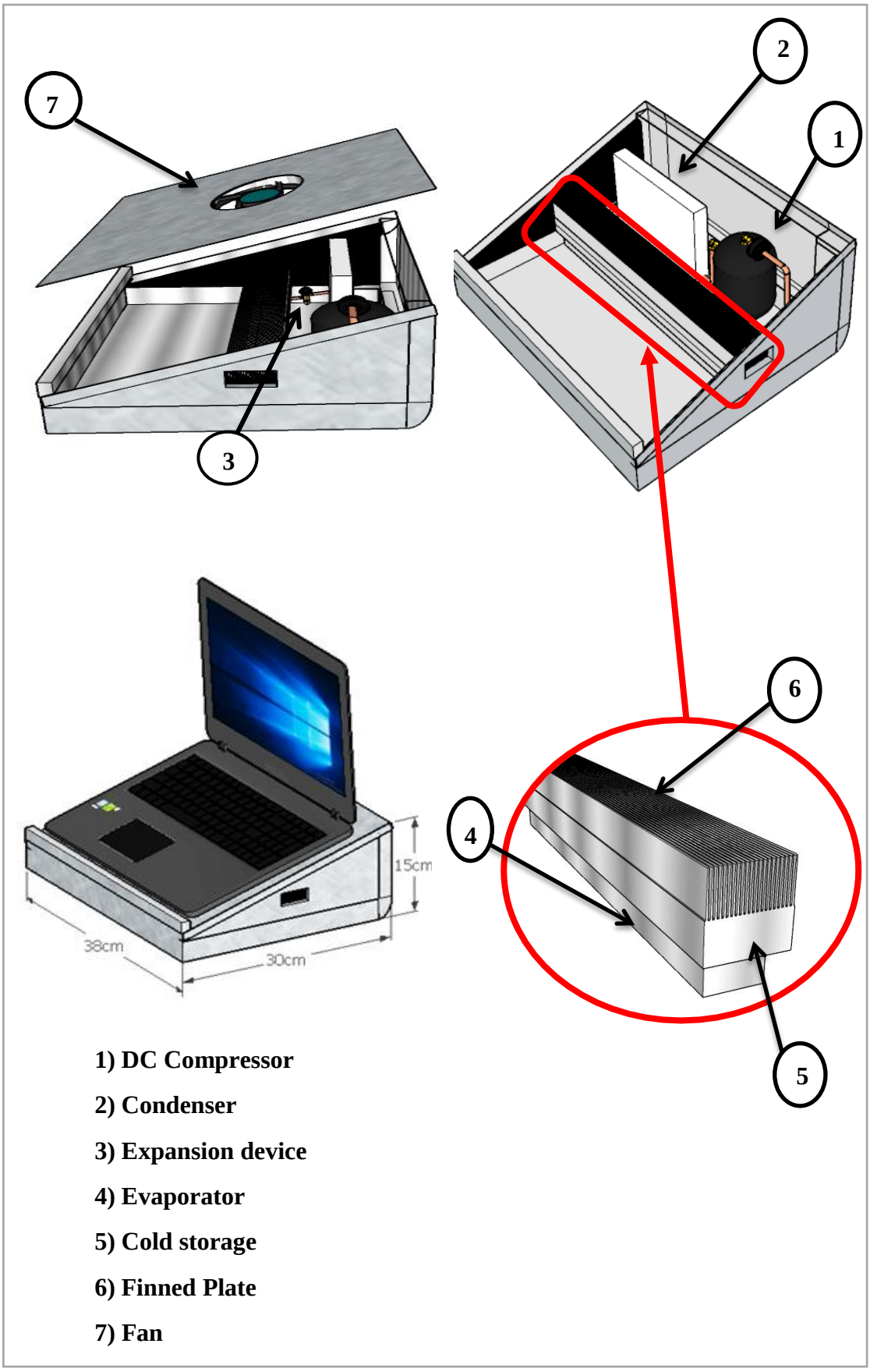

1) DC Compressor

2) Condenser

3) Expansion device

4) Evaporator

5) Cold storage

6) Finned Plate

7) Fan

Figure 3.3: The suggested design

3.5. Dimensions of The Cooling Stand

Figure 3.4 shows a side, front and 3d views of the Cooling stand that carry the system.

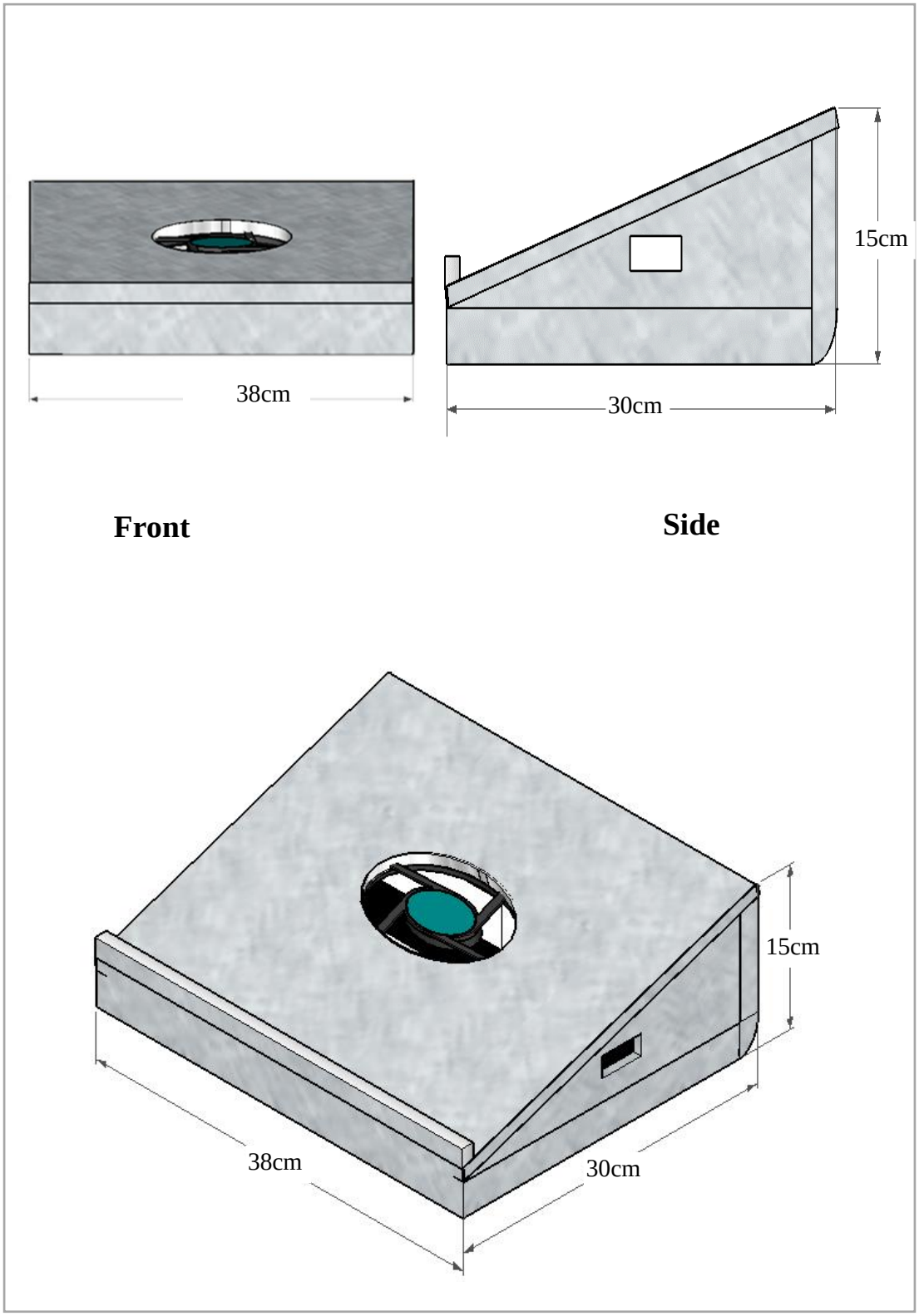

Figure 3.4: Side, front and 3d views of the Cooling stand

3.6. Dimensions of the Evaporator, Cold Storage and Finned Plate

Figure 3.5 shows a side, front and 3d views of the Evaporator, Cold Storage and Finned Plate.

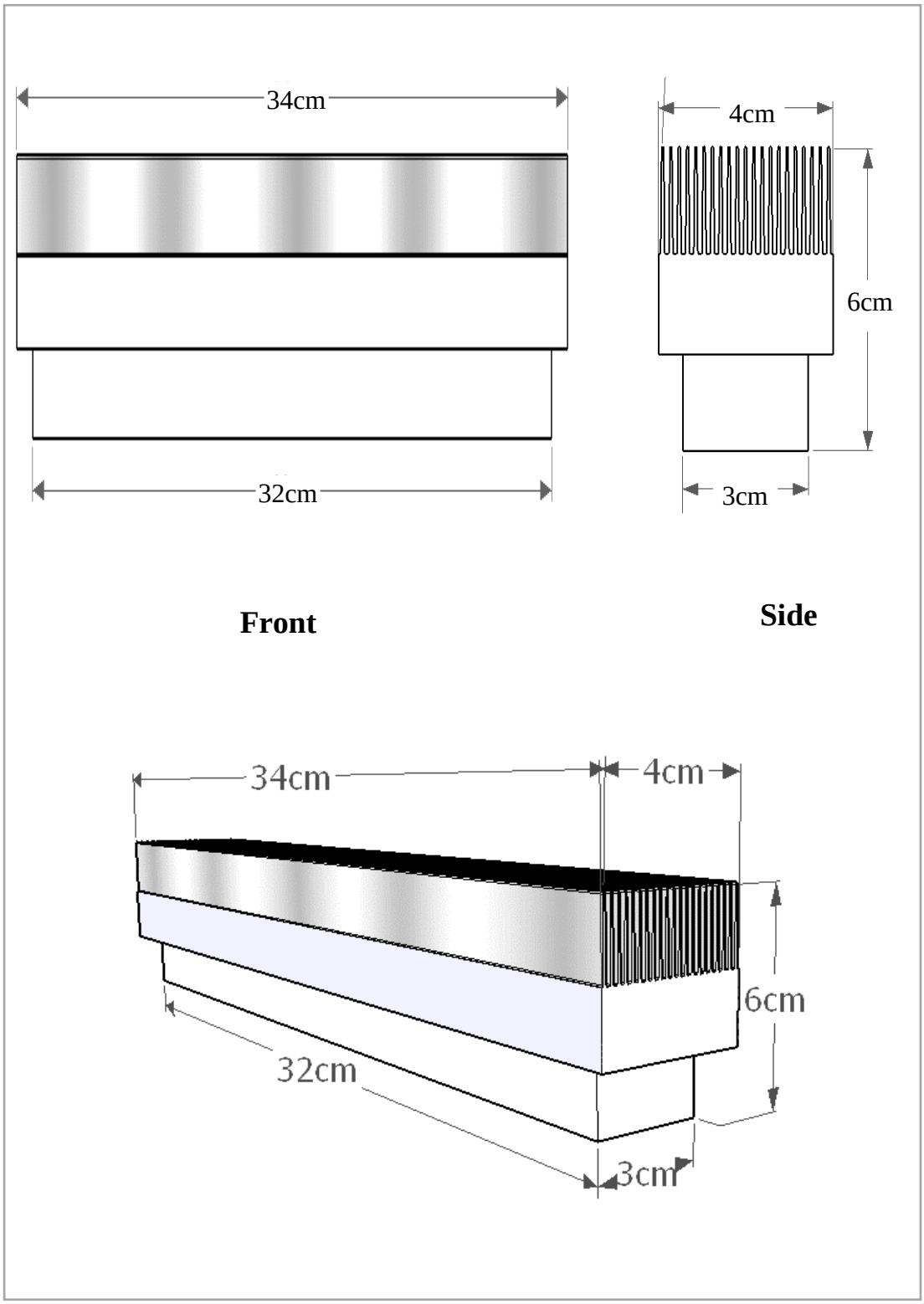

Figure 3.5: Side, front and 3d views of the Evaporator, Cold Storage and Finned Plate

3.7. Mathematical Formulation

In this section, we present the mathematical equations. The following assumptions are made about the system: 1) the sensible heat of PCM is neglected. 2) Heat loss from fluid and solid is neglected. 3) Heat transfer in the axial direction is only. 4) The properties of the fluids are constant.

3.7.1 Cooling performance. The cooling capacity ($\dot{Q}_e$) is assumed to be 100W and from that, we can calculate the mass flowrate of the working fluid ($\dot{m}_{ref}$) :

$$\dot{Q}_e = \dot{m}_{ref}(h_1 - h_4) \tag{1}$$

Where h_1 is the specific enthalpy of the refrigerant at the evaporator outlet (J/g), and h_4 is the specific enthalpy at the evaporator inlet (J/g).

The heating capacity, or the heat load of condenser ($\dot{Q}_C$), is the following:

$$\dot{Q}_c = \dot{m}_{ref}(h_2 - h_3) \tag{2}$$

Where h_2 and h_3 are the specific enthalpies at the inlet and outlet of the condenser (J/g), respectively.

The compressor power ($\dot{W}_{in}$):

$$\dot{W}_{in} = \dot{m}_{ref}(h_2 - h_1) \tag{3}$$

The Coefficient of Performance (COP) is used to evaluate the performance of the system under different refrigerants and is given below:

$$COP = \frac{\dot{Q}_e}{\dot{W}_{in}} \tag{4}$$

The second-law efficiency COP_{ex}can be writing as the following equation.

$$COP_{ex} = \frac{COP}{\frac{T_L}{(T_H - T_L)}} \tag{5}$$

Where T_L and T_H are the temperature of the evaporator (°C) and the temperature of the condenser (°C), respectively.

3.7.2 Cold storage. The energy storage of PCM (E_{stored}) can be modeled using the following equation:

$$E_{stored} = m_{PCM}L \tag{6}$$

Where m_{PCM} is the mass of PCM (g) and L is the specific latent heat of the PCM (J/g).

Chapter 4. Experimental Setup and Numerical Model

In this Chapter, we present the experimental setup for enhancing the thermal conductivity of bio-based PCM using Graphene Nanoplatelets (GNPs) and using Graphite, design of experiments, and numerical model of cooling performance of GnPs-PCM-based heat sink.

4.1. Experimental Setup for Enhancing the Thermal Conductivity of Bio-based PCM Using Graphene Nanoplatelets (GNPs)

4.1.1. Materials. The Bio-based PCM used in this experiment is obtained from Entropy Solutions, LLC. The PCM has a melting temperature of 29 °C and the heat required to melt 1 kg of this PCM is 202 kJ. Table 4.1 enlists the key thermal properties of the Bio-based PCM used in the experiment

Table 4.1 Thermal properties of PureTemp 29.

Property	Typical value
Phase Change Temperature	29 °C
Latent heat	202 kJ/kg
Specific heat capacity (solid)	1.77 kJ/ (kg · °C)
Specific heat capacity (liquid)	1.94 kJ/ (kg · °C)
Thermal conductivity (solid)	0.25 W/ (m · °C)
Thermal conductivity (liquid)	0.15 W/ (m · °C)
Density at 6 °C (solid)	0.94 g/cm3
Density at 30 °C (liquid)	0.85 g/cm3

The Graphene Nanoplatelets (Grade M) additive was used to enhance the thermal conductivity of the Bio-based PCM is supplied by XGScience. Table 4.2 summarizes the thermal properties of the interest of this GNP. On comparing the thermal conductivity between the PureTemp and the GNP, the vitality of the latter is realized as it largely enhances the thermal conductivity of the PCM.

Table 4.2: Key Thermal Properties of GnPs.

property	Typical value (perpendicular to surface)
Density	2.2 g/cm3
Thermal conductivity	6 W/ (m · °C)
Specific heat capacity	2.1 kJ/ (kg · °C)

4.1.2. Preparation of GNPs/Bio-based PCM composites. To mix the GNP with the PCM, the solid PCM was to be melted. Hence, the GNP was heated, above the prescribed melting point. After they were dissolved, the GnPs were mixed into the liquid PCM, with different Surfactants namely, sodium dodecyl sulfate (SDS), Sodium dodecylbenzene sulfonate (SDBS) and Sodium stearoyl lactylate (SSL). To ensure optimum dissolving and apt stirring, the mixture was ultra-sonicated using probe sonicator for 20 minutes. The sonicator setup, as visible in Figure 4.1, indicates the PCM-GNP sample mixture in a beaker and 500 W QSonica sonicator at a 25% amplitude. The mixture in the container to cool down and solidify at room temperature.

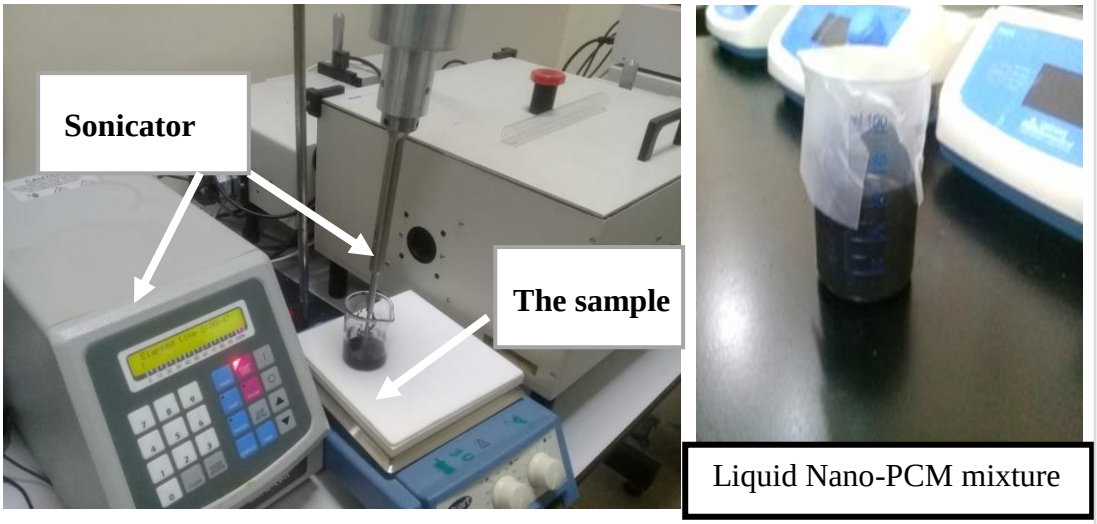

Figure 4.1: Preparation of GNPs/ PCM mixture

4.1.3. Thermal conductivity measurement. To measure the thermal conductivity of the samples of the pure bio-based PCM and Nano-PCM with different surfactants, a thermal conductivity analyzer from C-Therm Technologies was used. The measurements were taken at room temperature, about 25 °C. To minimize the effect of heat loss due to convection, a test cell with a small volume was extracted from the different samples. The test-cell is placed on the sensor to take the readings, as visible in Figure 4.2, after the sample solidified.

4.1.4 Latent heat measurement. In the measurement of the latent heat of the pure bio-based PCM and the three Nano-PCM's with different surfactants, a Differential Scanning Calorimeter (DSC- 60a Plus, Shimadzu), as visible in Figure 4.3, was used. The latent heats of the four samples including the pure PCM are analyzed

and then compared using the DSC analysis. Thus, it is possible to assess the effect each surfactant imposes on the latent heat. In the current DSC analysis, an initial reference temperature of 24 °C was used in all samples. The samples are then heated with a heating rate of 1°C/min until they reached a temperature of 45°C after the analysis. In the current experiment, only the melting process (endothermic process) is analyzed.

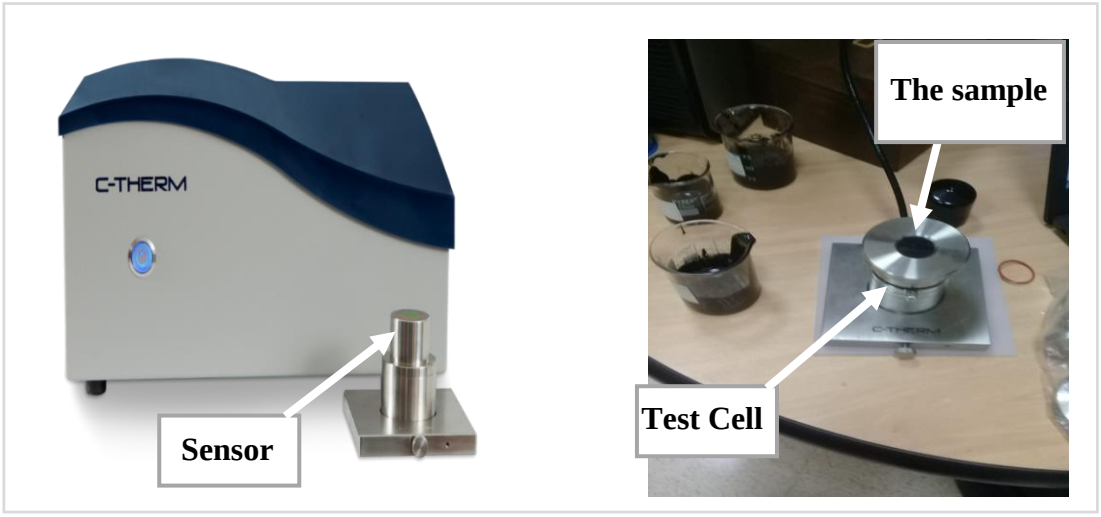

Figure 4.2: C-Therm Thermal Conductivity Analyzer

Figure 4.3: Shimadzu DSC-60a Plus Differential Scanning Calorimeter

4.1.5 Experimental setup. To evaluate the performance of the PCM-GNP mixture as a heat sink, the TecQuipment Free and Forced Convection Experimental Apparatus was utilized. As seen in Figure 4.4, the setup is used to measure the heater surface temperature. The heated surface on the setup with dimensions of 106 x 106 x 3 mm3 dissipates heat to the aluminum container consisting of the 30 mL mixture. Temperature is measured using a thermocouple on the aluminum plate on which the mixture container is kept. The heater that transmits heat to the plate is set to a power of

10W. To record and analyze the temperature and heat transfer data of interest, data acquisition system is used.

A schematic diagram of a cross-section of the PCM-based heat sink is presented in Figure 4.5. A constant heat flux of 943 W/m2 was applied to the bottom wall of the plate.

Figure 4.4: Experimental Apparatus

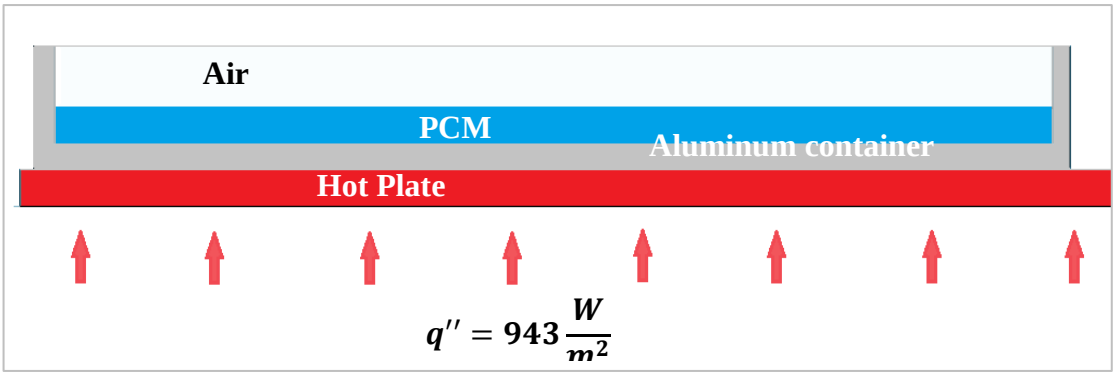

Figure 4.5: Schematic diagram of the cross-section of PCM based heat sink.

4.2. Experimental Setup for Enhancing The Thermal Conductivity of Bio-based PCM Using Graphite

4.2.1. Materials. For the current experiment, the PCM used was characterized by a melting temperature of 29 °C and an enthalpy of fusion of 202 KJ/Kg. The bio-based PCM used was acquired from Entropy Solutions, LLC. Table 4.3 summarizes all-important thermal properties with regards to the PCM used in the experiment.

As for the conductive-additive used, graphite flakes with 500 mesh size was used to improve the thermal conductivity of the PCM. It is important to observe that the thermal conductivity of Graphite is much larger than the thermal conductivity of the PCM as it ranges from 25-470 W/ (m · °C) due to the anisotropy of its layers compared to 0.15 W/ (m · °C) of the PCM, thus the choice to use Graphite as an additive to improve the thermal conductivity of the bio-based PCM is justified.

Table 4.3: Thermal properties of PureTemp 29.

Property	Typical value
Phase Change Temperature	29 °C
Latent heat	202 kJ/kg
Specific heat capacity (solid)	1.77 kJ/ (kg · °C)
Specific heat capacity (liquid)	1.94 kJ/ (kg · °C)
Thermal conductivity (solid)	0.25 W/ (m · °C)
Thermal conductivity (liquid)	0.15 W/ (m · °C)
Density at 6 °C (solid)	0.94 g/cm3
Density at 30 °C (liquid)	0.85 g/cm3

4.2.2 Preparation of Graphite /Bio-based PCM composites. In order for the Graphite to be effectively mixed with the solid PCM, it is required that the PCM be melted into a liquid state by increasing the temperature of the PCM above the melting point. The second step is to adequately mix the Graphite particles within the PCM to form a continuous homogeneous mixture. Next, Surfactants were combined with the Graphite -PCM mixture. Three different samples each containing one of three different Surfactants namely; Sodium dodecyl sulfate (SDS), Sodium dodecylbenzene sulfonate (SDBS) or Sodium stearoyl lactylate (SSL) were formed. A probe sonicator was employed for a period of around 20 minutes to ensure thorough dissolving and adequate stirring via the ultra-sonication process. The PCM- Graphite sample mixtures were then spread onto a beaker and re-sonicated using a 500W sonicator at 25% power. Each sample was then allowed to solidify at room temperature. Figure 4.6 provides a visual of the sonicator setup and the liquid PCM- Graphite mixture.

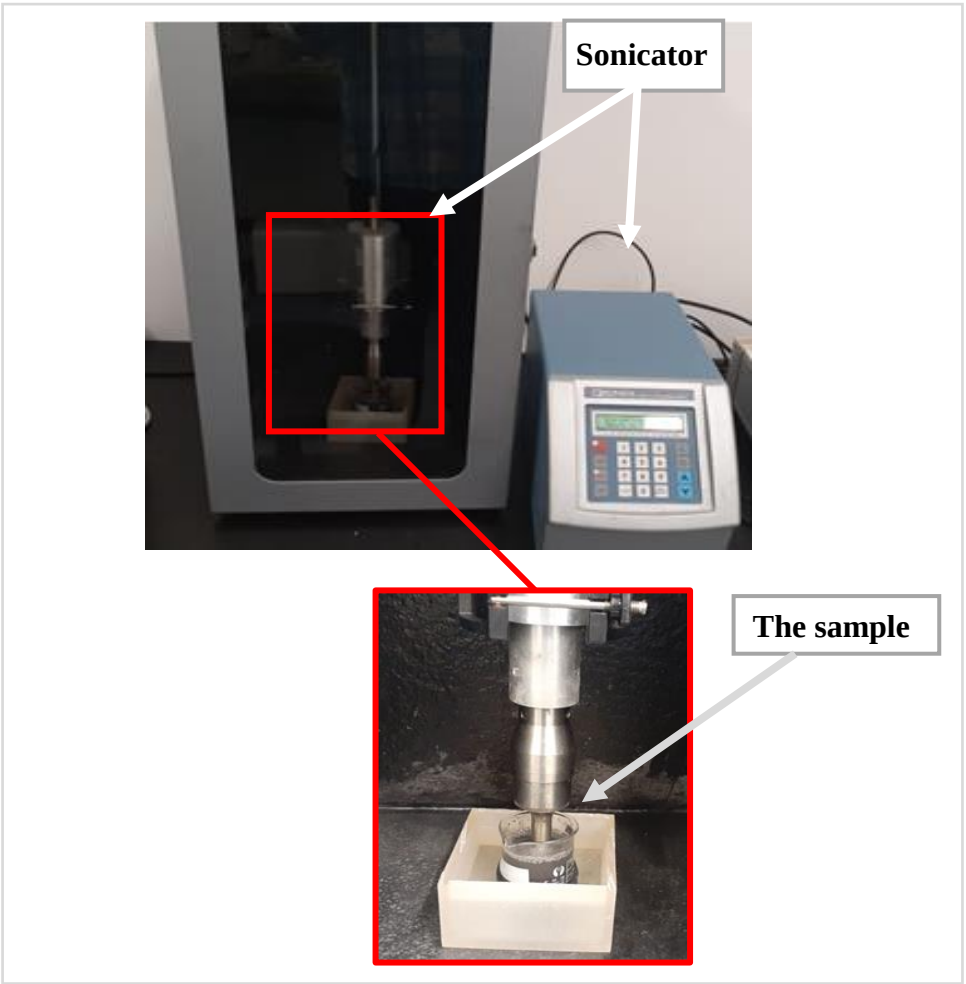

Figure 4.6: Preparation of Graphite/ PCM composites

4.3. Measurement Error Analysis

As illustrated by Table 4.4, the resolution of each instrument is adequately accurate to not cause any validation issues. The heaters are the least accurate component, however, the heaters in such research do not need high accuracy. The thermocouple and the balance measure data to a high accuracy, have a good resolution and minor uncertainties. The TecQuipment Free and Forced convection experiment provided sufficient accuracy as a ±0.2°C temperature uncertainty maintains the validity and integrity of temperature data.

Table 4.4: Instrument Uncertainty

Instrument	Uncertainty	deviation (Precision)
C-Therm TCi thermal conductivity analyzer	±0.01 W/m K	0.02 W/m K
Q500 QSonica sonicator	-	1 W
Citizen CX220 Analytical Balance	±0.1 mg	0.1mg
TecQuipment experiment (Heater) [Model: TD1005]	±0.1W	1W
TecQuipment experiment (Thermocouple) [Model: TD1005]	±0.2°C	0.1°C
Shimadzu DSC-60a Plus	±0.01 mW	0.01 mW

4.4. Design of Experiments (DoE)

The one of the main objectives of this research is to establish the best surfactant for the NanoPCM that can be used as a thermal storage medium, and the suitable carbon additive-surfactant ratio.

DoE is concerned with investigating the relationship between independent and dependent variables, where the independent variables are the type of Surfactant, the mass fraction of the carbon additive and carbon additive-surfactant ratio, and the dependent variables are the thermal conductivity (K) of the mixture, and the time taken to reach the reference temperature.

Table 4.5 shows the design of experiments for GnPs-PCM mixtures, where the independent variables are the type of Surfactant, the mass fraction of the GnPs, while Table 4.6 shows the design of experiments for Graphite -PCM mixtures, where the type of Surfactant, the mass fraction of the Graphite, and Graphite -surfactant ratio are the independent variables

Table 4.5: The Design of Experiments for GnPs-PCM mixtures

Input Factors							**Output measures**	
constant		**Independent Variable**					**dependent Variable**	
Input Power	10 W	Sample #	Surfactant Type	PCM (wt %)	GnPs (wt %)	Sur (wt %)	Time (sec)	K $(\frac{W}{m.K})$
		1	-	100	0	0	TBM	TBM
		2	SDS	98	1	1	TBM	TBM
		3	SDBS	98	1	1	TBM	TBM
		4	SSL	98	1	1	TBM	TBM
		5	SDS	94	3	3	TBM	TBM
Volume	30 ml	6	SDBS	94	3	3	TBM	TBM
		7	SSL	94	3	3	TBM	TBM
		8	SDS	90	5	5	TBM	TBM
		9	SDBS	90	5	5	TBM	TBM
		10	SSL	90	5	5	TBM	TBM

Note. “TBM” stands for “To Be Measured”.

.

Table 4.6: The Design of Experiments for Graphite-PCM mixtures

Input Factors							**Output measures**	
constant		**Independent Variable**					**dependent Variable**	
Input Power	10 W	Sample #	Surfactant Type	PCM (wt %)	Graphite (wt %)	Sur (wt %)	Time (sec)	K $(\frac{W}{m.K})$
		1	-	100	0	0	TBM	TBM
		2	SDS	96	1	3	TBM	TBM
		3	SDBS	96	1	3	TBM	TBM
		4	SDS	95	1	4	TBM	TBM
		5	SDBS	95	1	4	TBM	TBM
Volume	30 ml	6	SDS	94	1	5	TBM	TBM
		7	SDBS	94	1	5	TBM	TBM
		8	SDS	88	3	9	TBM	TBM
		9	SDBS	88	3	9	TBM	TBM
		10	SDS	85	5	15	TBM	TBM
		11	SDBS	85	5	15	TBM	TBM

Note. “TBM” stands for “To Be Measured”.

4.5. Numerical Model of Cooling Performance of GnPs-PCM-Based Heat Sink

ANSYS Fluent software was used to simulate an aluminum container with dimensions of 110 x 100 x 10 mm as the heat sink containing 30 ml of either pure bio-PCM or Nano-PCMs. The same material properties that were used in the experimental

setup were also used in the numerical analysis. The properties of the PCM and GnPs are listed in Table 4.1 and Table 4.2, respectively. The analysis assumed that the Nano-PCM mixture was homogeneous. It also took into account the convective heat transfer on the surface as the PCM was exposed to the air. A schematic diagram of a cross-section of the PCM-based heat sink is presented in Figure 4.5. A constant heat flux of 943W/m2 was applied to the bottom wall of the plate. Figure 4.7 shows the flow chart of CFD analysis process.

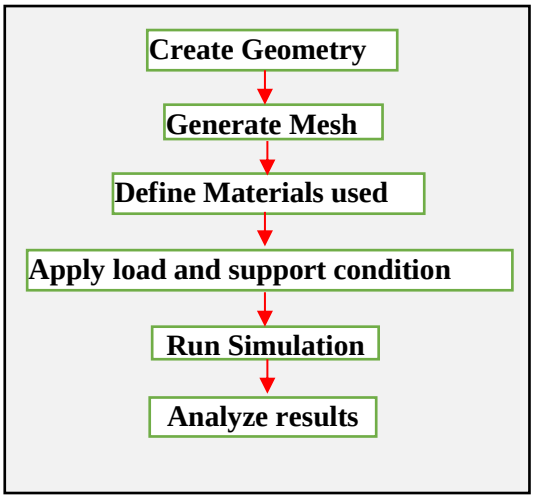

Figure 4.7: Flow chart for CFD analysis

4.5.1. Governing equations: The governing equations of the model are:

Continuity equation:

$$\nabla.(\rho\vec{V}) = 0 \tag{7}$$

Where ρ is the density of the fluid (kg/m3), and $\vec{V}$ is the velocity (m/s) of the fluid.

Momentum equation:

$$\frac{\partial(\rho\vec{V})}{\partial t} + \nabla.(\rho\vec{V}\vec{V}) = -\nabla.P + \rho\vec{g} + \nabla.\vec{\tau} + \vec{F} \tag{8}$$

Where $t, P, \vec{g}, \vec{\tau}, \vec{F}$ are the time (s), the pressure of the fluid, gravitational acceleration stress, and force.

Energy equation:

$$\frac{\partial(\rho h)}{\partial t} + \nabla.(\rho\vec{V}h) = \nabla.(K\nabla T) \tag{9}$$

Where K is the thermal conductivity (w/m. K), and T is the temperature of fluid.

4.5.2. Model selection:

- Transient State.
- Energy- On.
- Melting – On.
- The flow is incompressible and laminar.
- Nano-PCM mixture is homogeneous.
- 3D model is used.

4.5.3. Thermal properties: The thermal conductivity in solid phase is obtained from experimental data. The density (ρ), specific heat capacity (C_p) of the Nano-PCM are calculated from the following equations:

$$\rho_{nanoPCM} = x\rho_{nano} + (1-x)\rho_{PCM} \tag{10}$$

$$C_{p_{nanoPCM}} = \frac{x(\rho_{nano}C_{p_{nano}})+(1-x)(\rho_{PCM}C_{p_{nanoPCM}})}{\rho_{nanoPCM}} \tag{11}$$

Where x is the mass fraction of the nanoparticles.

4.5.4. Mesh independence study: Figure 4.8 shows the temperature of the heater at time=450s versus four different mesh sizes (0.005, 0.003, 0.001, and 0.0005 mm). Analysis of the first mesh was conducted in the first simulation then the temperature of the heater with time=450s was recorded, after that the analysis was done with finer mesh with the same boundary conditions and computation time. Since the solution is stable with the refinement mesh, the first mesh was selected to reduce the computation time.

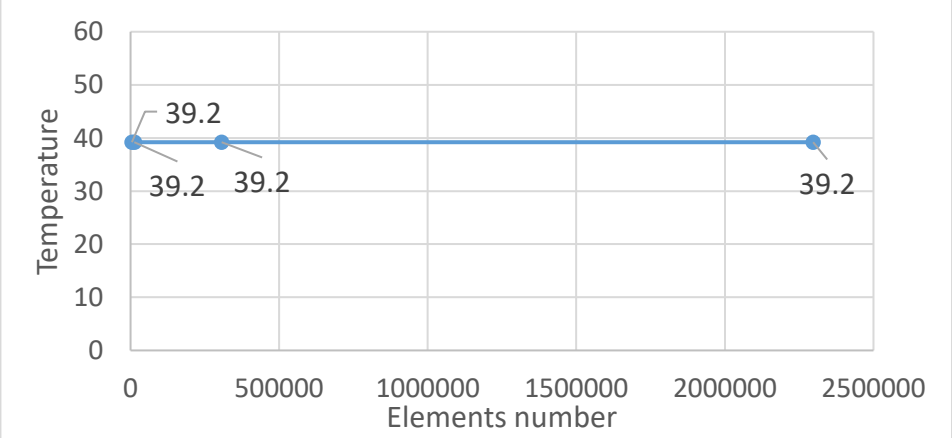

Figure 4.8: Mesh independence test.

Chapter 5. Results and Analysis

The thermal performance of bio-based PCM with GnPs and Graphite integrated into a heat sink, heat transfer analysis of PCM-based heat sink, thermal responses of the CPU, and comparison between experimental and numerical results are presented in this chapter.

5.1. Operating Conditions of the System

The design operating conditions of the system were chosen to charge the PCM, where the design cooling capacity is 100 W. Table 5.1 presents the operating conditions for the proposed system.

Table 5.1: Operating conditions for the proposed system

Parameter	Assigned value
Cooling capacity	100 W
Condenser temperature	35 °C
Compressor efficiency	0.8

5.2. Choice of Refrigerant

Figures 5.1, 5.2, 5.3, 5.4, 5.5, and 5.6 show the effect of evaporator temperature on the Energetic Coefficient of Performance (COP_{en}) for different refrigerants at the discharge temperature of 40°C, 50°C, 60°C, 70°C, 80°C, and 90°C, respectively. As the evaporator temperature increases, the energetic coefficient of performance increases. It is also found that R134a has the best performance among the others at different discharge temperatures and different evaporator temperatures. The maximum COP_{en} for R13a4, R600a, and R404a at the discharge temperature of 40°C were reported as 5.4, 4.1and 5.0, respectively.

The effect of evaporator temperature for different refrigerants on the Exegetic Coefficient of Performance (COP_{ex}) at the discharge temperature of 40°C, 50°C, 60°C, 70°C, 80°C, and 90°C are shown in Figures 5.7, 5.8, 5.9, 5.10, 5.11, and 5.12, respectively. It is noted that the Exegetic Coefficient of Performance decreases with increasing the evaporator temperature.

R134a is the best option to choose as the working fluid since it has the highest COP. The refrigerant requires the lowest power consumption for the proposed system

as shown in Table 5.2. The parameter values were calculated using EES software based on the above operating conditions.

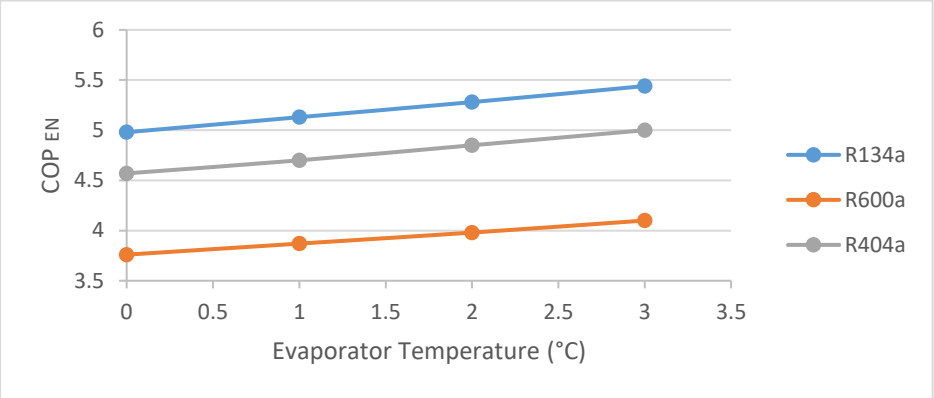

Figure 5.1: The effect of evaporator temperature on the energetic coefficient of performance (COP_{en}) for different refrigerants at the discharge temperature of 40°C

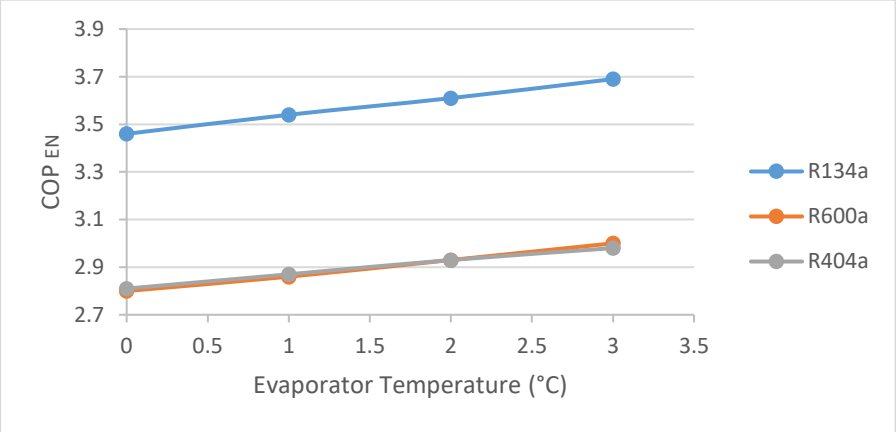

Figure 5.2 : The effect of evaporator temperature on the energetic coefficient of performance (COP_{en}) for different refrigerants at the discharge temperature of 50°C

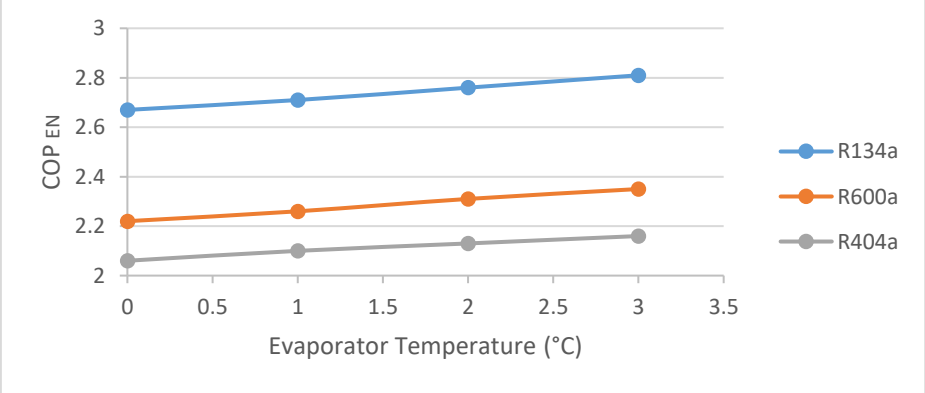

Figure 5.3: The effect of evaporator temperature on the energetic coefficient of performance (COP_{en}) for different refrigerants at the discharge temperature of 60°C

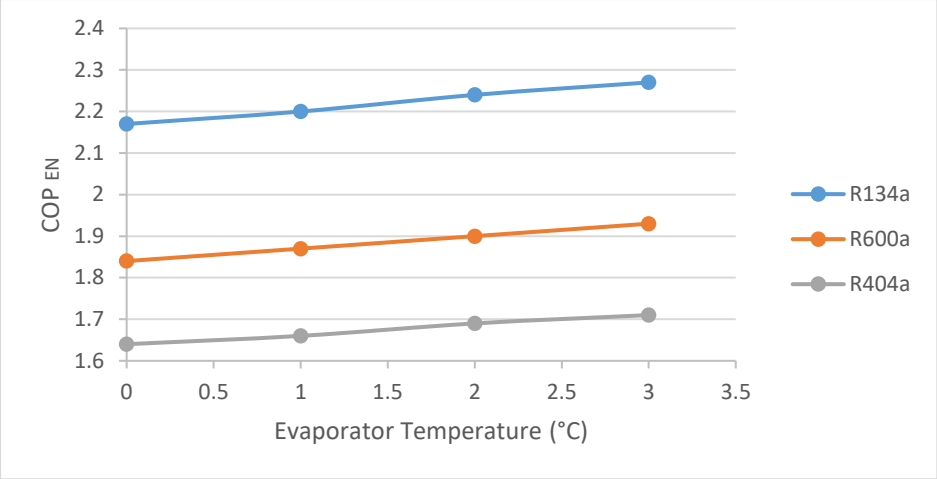

Figure 5.4: The effect of evaporator temperature on the energetic coefficient of performance (COPen) for different refrigerants at the discharge temperature of 70°C

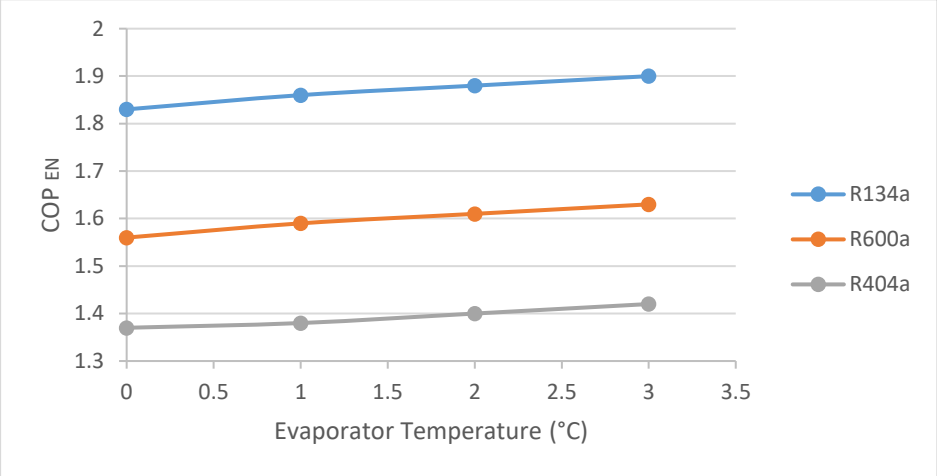

Figure 5.5: The effect of evaporator temperature on the energetic coefficient of performance (COP_{en}) for different refrigerants at the discharge temperature of 80°C

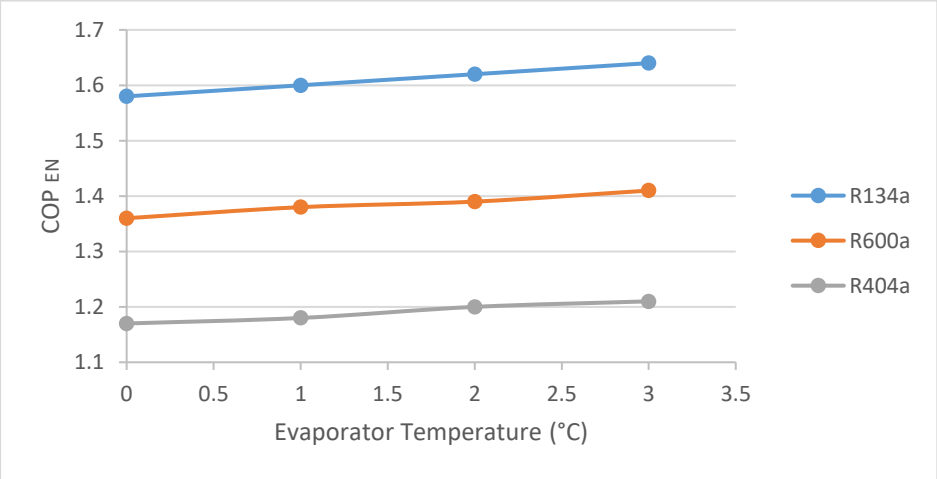

Figure 5.6: The effect of evaporator temperature on the energetic coefficient of performance (COPen) for different refrigerants at the discharge temperature of 90°C

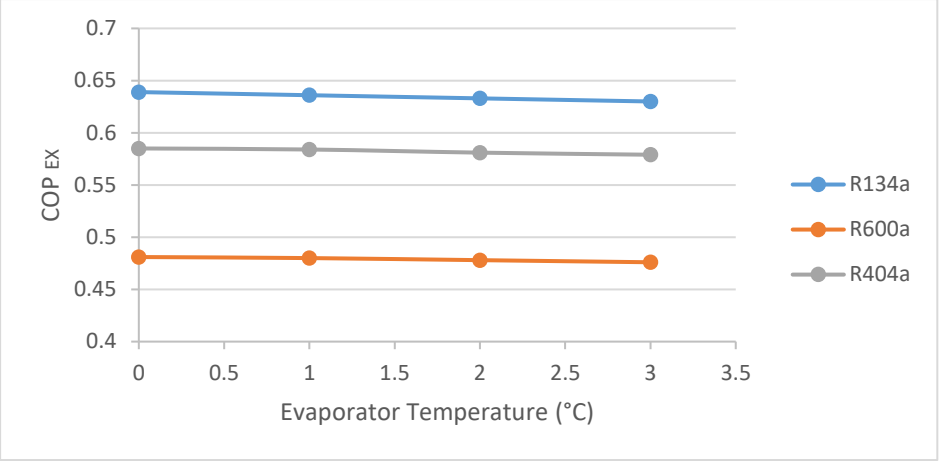

Figure 5.7: The effect of evaporator temperature on the Exegetic Coefficient of Performance (COPex) for different refrigerants at the discharge temperature of 40°C

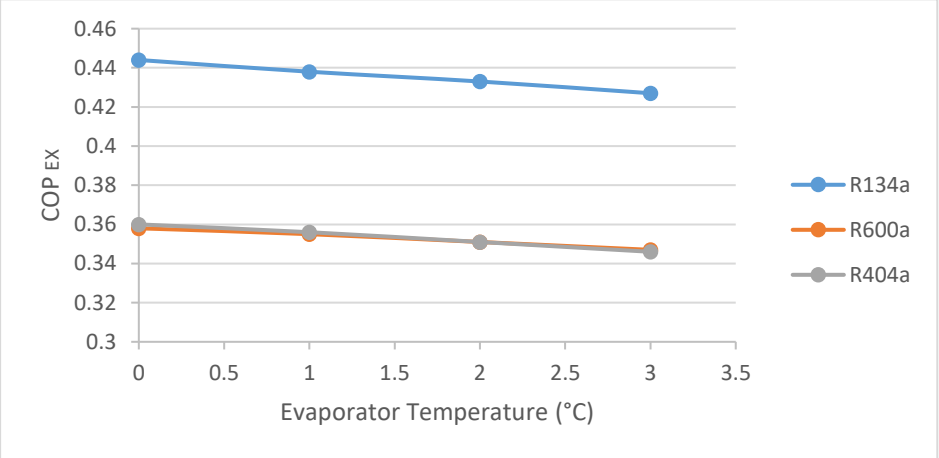

Figure 5.8: The effect of evaporator temperature on the Exegetic Coefficient of Performance (COPex) for different refrigerants at the discharge temperature of 50°C

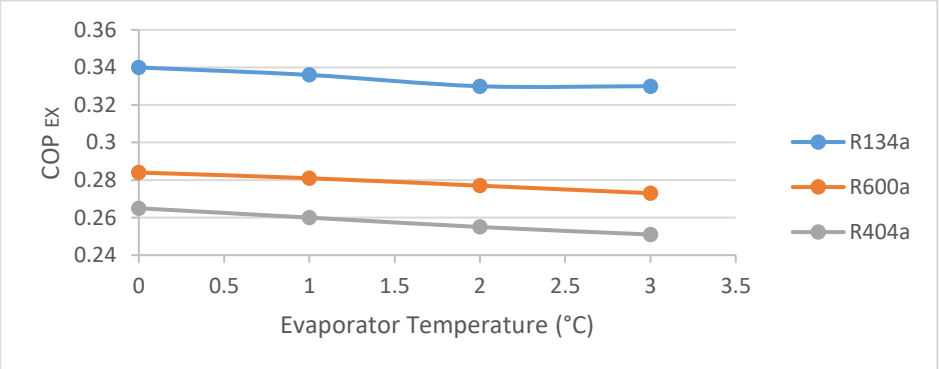

Figure 5.9: The effect of evaporator temperature on the Exegetic Coefficient of Performance (COPex) for different refrigerants at the discharge temperature of 60°C

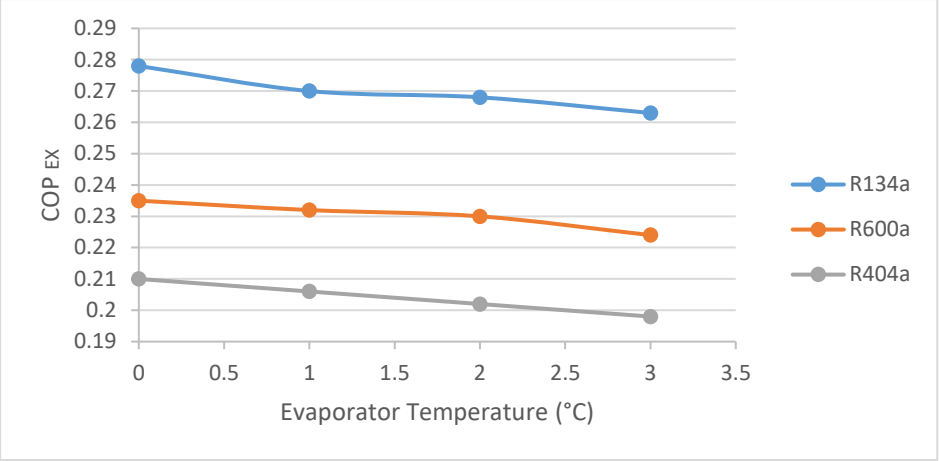

Figure 5.10: The effect of evaporator temperature on the Exegetic Coefficient of Performance (COPex) for different refrigerants at the discharge temperature of 70°C

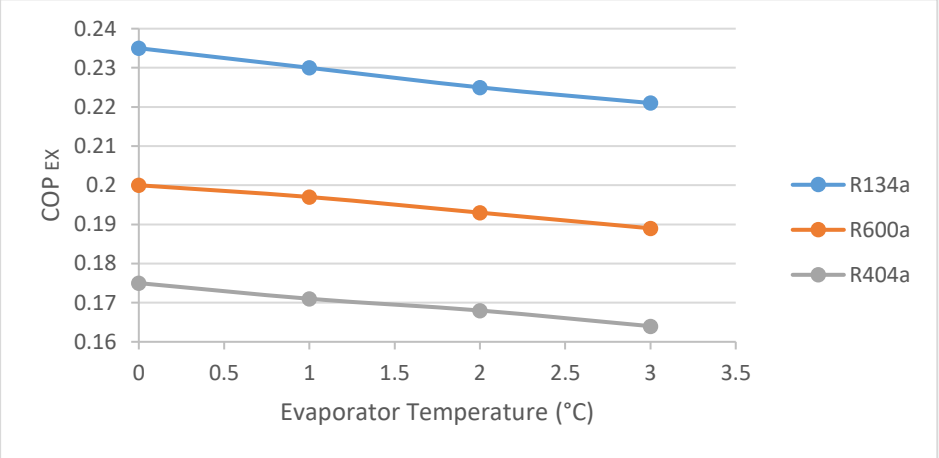

Figure 5.11: The effect of evaporator temperature on the Exegetic Coefficient of Performance (COPex) for different refrigerants at the discharge temperature of 80°C

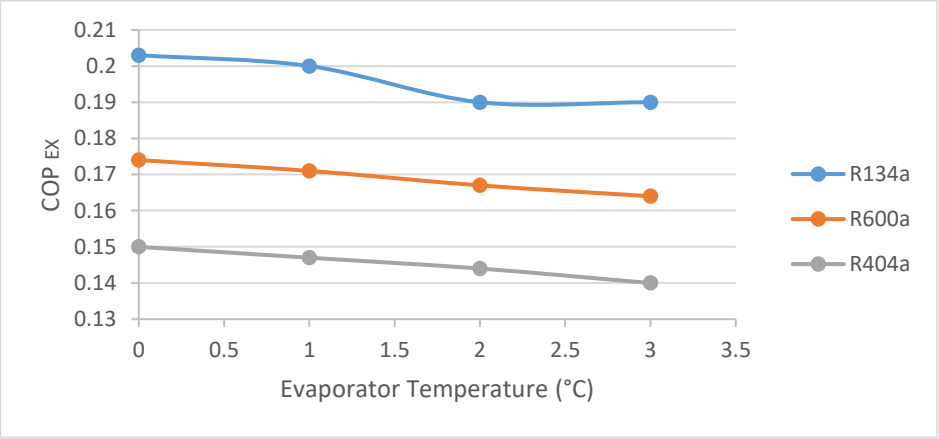

Figure 5.12: The effect of evaporator temperature on the Exegetic Coefficient of Performance (COPex) for different refrigerants at the discharge temperature of 90°C

5.3. Operating Conditions of the System Using R134a as a Refrigerant

The design operating conditions of the system using R134a as a refrigerant are listed in Table 5.2

Table 5.2: Operating conditions for the proposed system

Parameter	Value
Cooling capacity	100 W
Evaporator pressure	0.30 MPa
Superheated at the condenser inlet	60 °C
Mass rate	0.67 g/s
Condenser pressure	0.89 MPa
Pressure ratio	2.9
COP	2.71

5.4. The Thermal Responses of the CPU

Figure 5.13 shows the effect of using the laptop cooler on the CPU temperature that starts at 64°C. In the period time of 600 sec, each condition of the experiment was performed at a room temperature of 24°C. To control the power of the CPU and to run it for an extended length of time, PowerMax software that is a CPU burn-in test was used. In addition, HWMonitor, a hardware-monitoring program, was used to read the voltage and the temperature of the laptop.

When the laptop cooler was used, the maximum CPU temperature was found to be 67 °C, while it was 78 °C without using the cooler. Noticeably, when the cooler was used that helped in reducing the temperature of CPU by 11 degrees (14.1%), the temperature of the CPU was more suppressed.

Figure 5.14 shows the variation of the overall heat transfer coefficient with time. Using the cooler, a higher heat transfer coefficient is obtained (339 W/ $(m^2 K)^{-1}$). The overall heat transfer coefficient was increased by 28.5% because the air entering the laptop was cooled down using the laptop cooler and the flow rate of the air was increased.

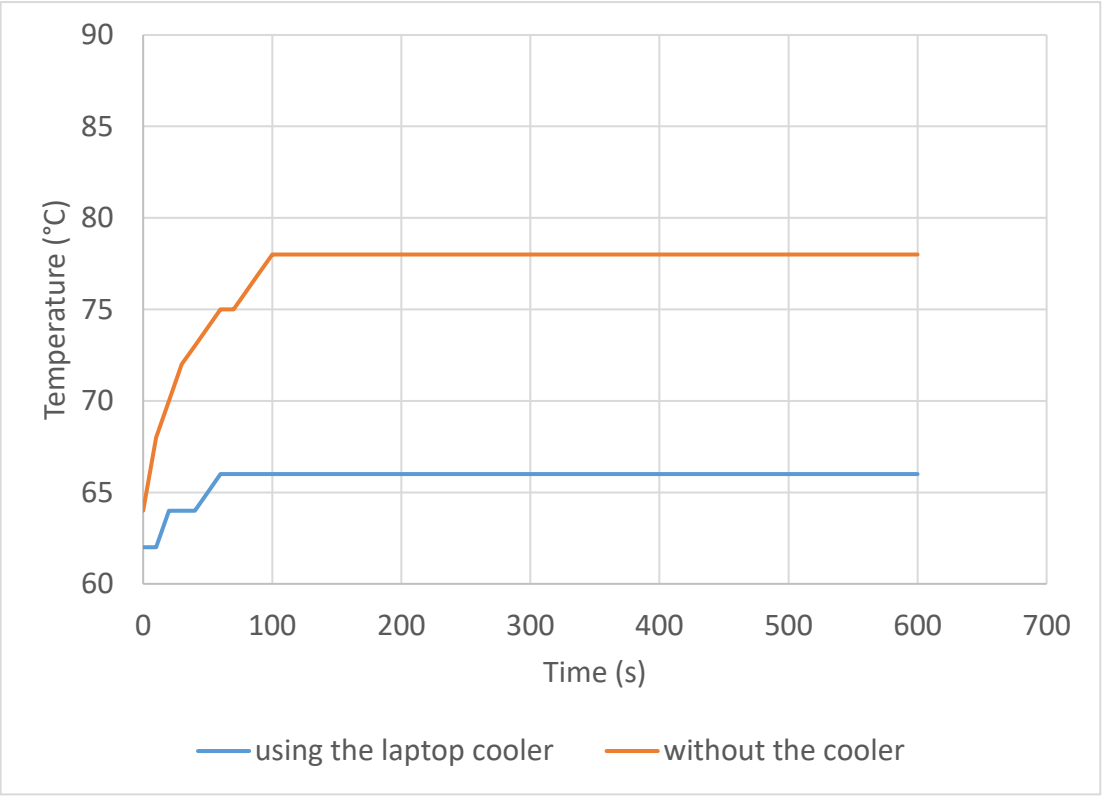

Figure 5.13: The thermal responses of the CPU at 20W power

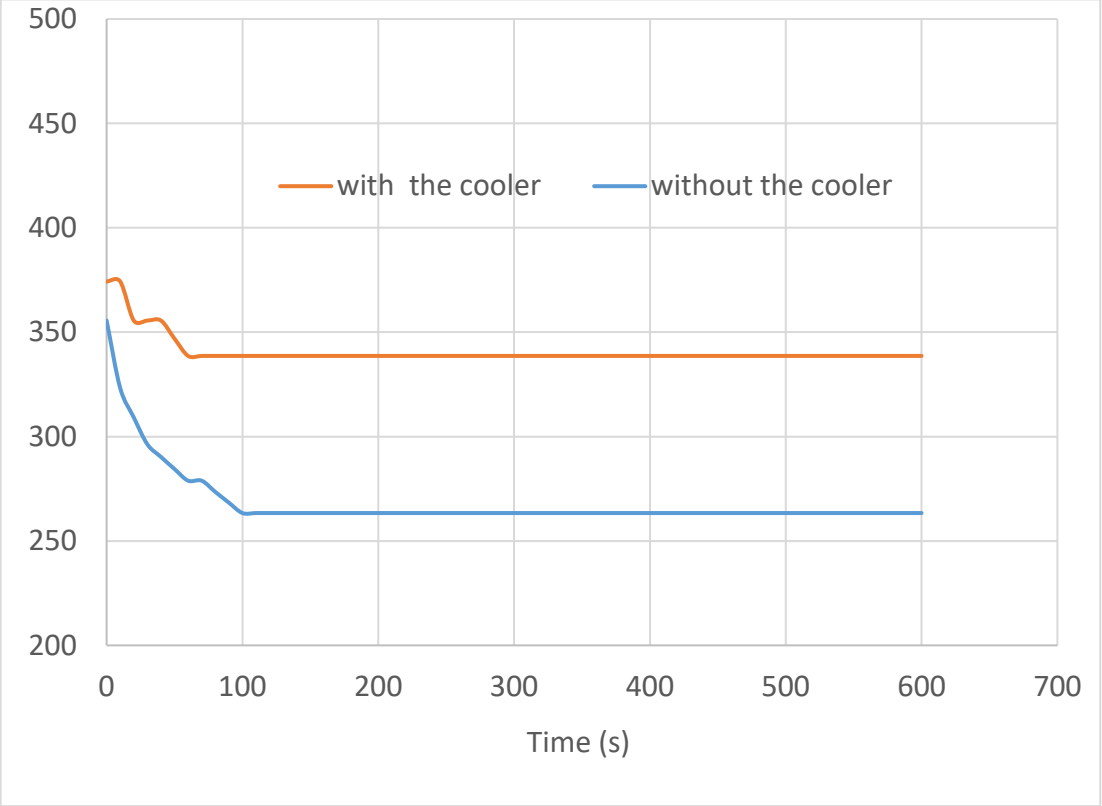

Figure 5.14: The variation of the overall heat transfer coefficient with time

5.5. Thermal Conductivity of GnPs/Bio-based PCM Composites

Figure 5.15 describes the results of the thermal conductivity experiments in the case of PurePCM as well as the case of 1%, 3% and 5% mass fractions for GnPs along with each of the three surfactants considered.

Firstly, the results affirm that the addition of a GnP-Surfuctant mixture into the PurePCM allows for the improvement of the thermal conductivity of the PCM. PurePCM reported a maximum thermal conductivity of 0.22 W/ (m. K) whilst the GnP-Surfuctant mixed, PCM reported significantly higher values for the thermal conductivity. The maximum thermal conductivity measured for 1%, 3%, and 5% GnPs mass fractions were reported as 0.544 W/ (m. K), 0.79 W/ (m. K) and 1.03 W/ (m. K), respectively. These numbers correspond to a thermal conductivity increase of nearly 150%, 260%, and 370% for the 1%, 3%, and 5% GnPs mass fractions, respectively. It is important to recognize that in all cases (1%, 3%, 5% GnPs mass fractions) NanoPCM SDS exhibited the maximum thermal conductivity followed closely by NanoPCM SDBS.

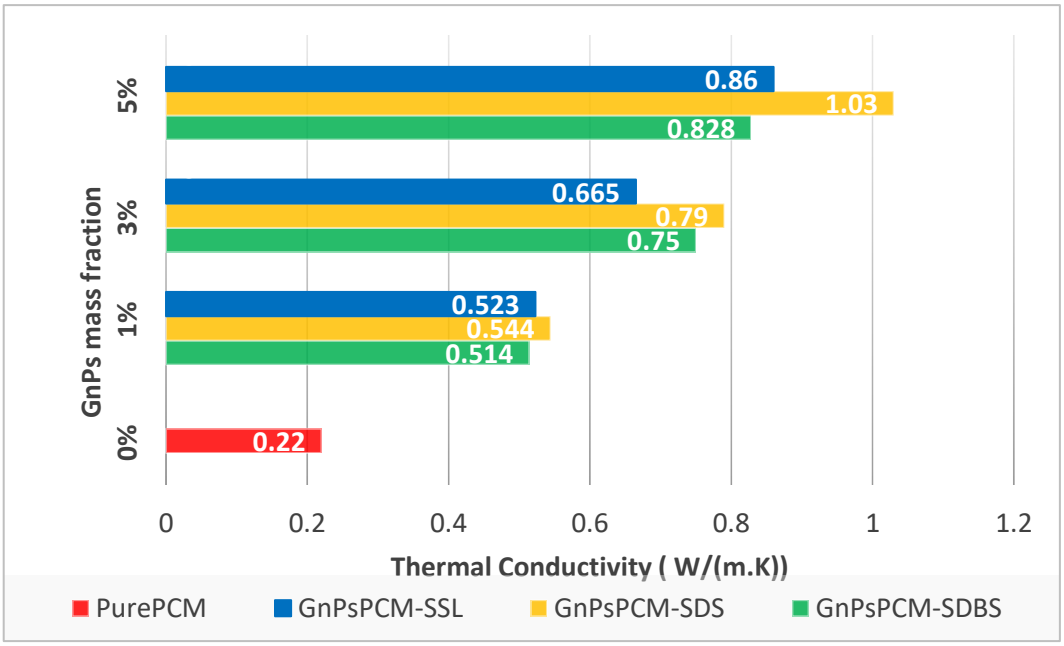

Figure 5.15: Thermal conductivity values for GnPs-PCM with different GnPs mass fractions and surfactant

Amongst the studied GnPs mass fractions, the 5% mass fraction reported the highest thermal conductivity value. If the NanoPCM SDS measurement is compared amongst the three cases, we can see that the 5% mass fraction reported a thermal conductivity of 1.03 W/ (m. K) whilst the 3% and 1% mass fraction reported values of

0.79 and 0.544 W/m.K, respectively. These values represent a positive percentage difference between the 5% and 3% of 26% and a positive percentage difference between the 5% and 1% of 62%. A similar trend is observed in the case of the NanoPCM-SDBS and the NanoPCM-SSL.

5% GnPs mass fraction NanoPCM-SDS reports the maximum thermal conductivity value and is thus the best alternative amongst the experimented materials.

5.6. DSC Analysis of GnPs/Bio-based PCM Composites

The investigated phase change enthalpy values from the DSC analysis are presented in Figure 5.16. The analysis was carried out for the three Nano-PCM samples as well as the Pure Bio-based PCM. The Pure PCM produced a Phase Change enthalpy value of 212.2 J/g whilst the NanoPCM-SDS, NanoPCM-SDBS, and NanoPCM-SSL demonstrated phase change enthalpy values of 145.9, 206.7 and 236.5 J/g respectively. From these values, it is possible to infer that the NanoPCM-SDS and NanoPCM-SDBS varieties exhibited a decreased phase change enthalpy of 31% and 2.6 %, respectively when compared to the pure PCM. The NanoPCM-SSL on the other hand exhibited an increase in phase change enthalpy by a value of 11.5% when compared to the Pure-PCM. Thus, when phase change enthalpy is considered it is possible to conclude that SSL surfactant along with the Nano additive improves the phase change enthalpy of pure bio-based PCM and is thus the best candidate in this regard. Figures 5.17-5.20 show the DSC analysis of Pure PCM the NanoPCM-SDS, NanoPCM-SDBS, and NanoPCM-SSL, respectively.

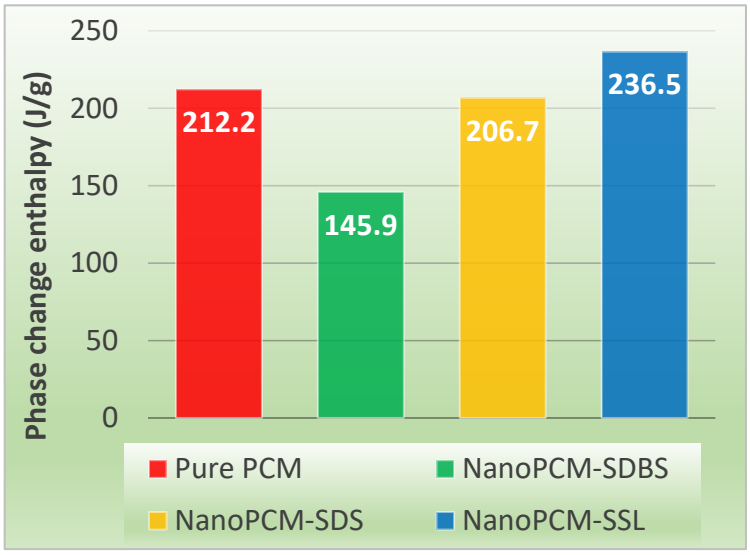

Figure 5.16: Phase Change enthalpy values of the investigated samples

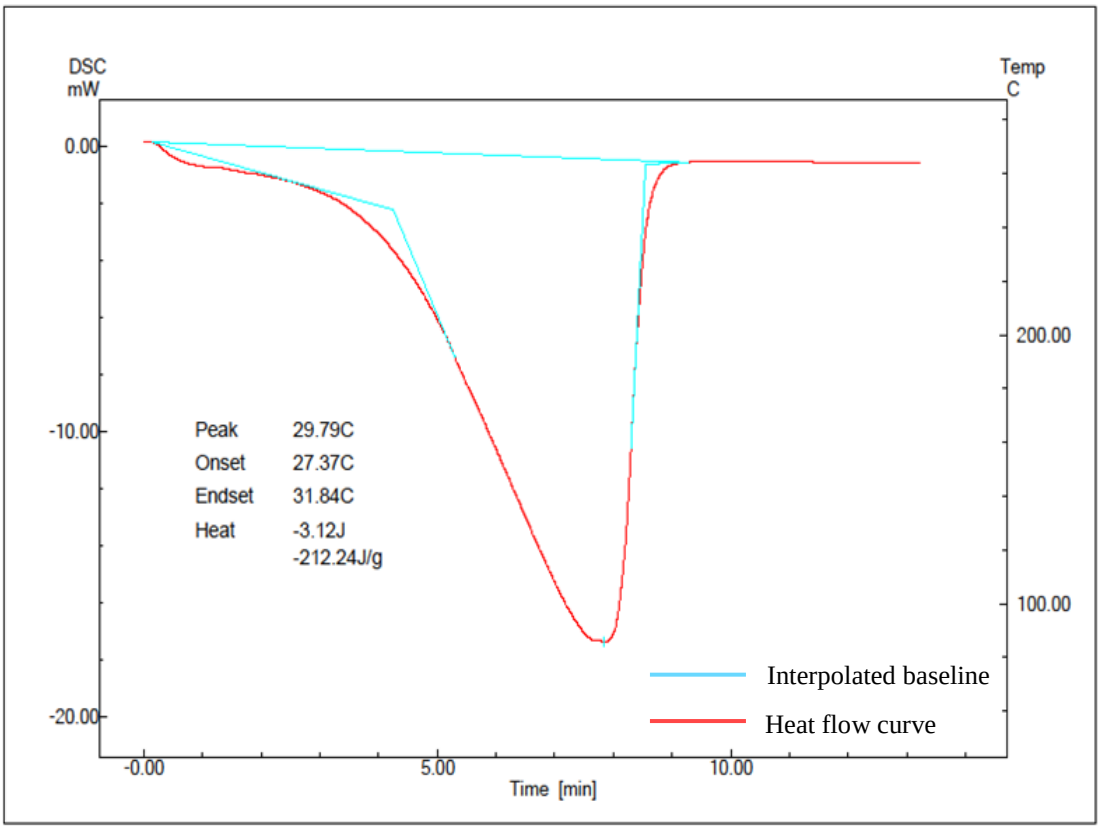

Figure 5.17: DSC analysis of Pure PCM

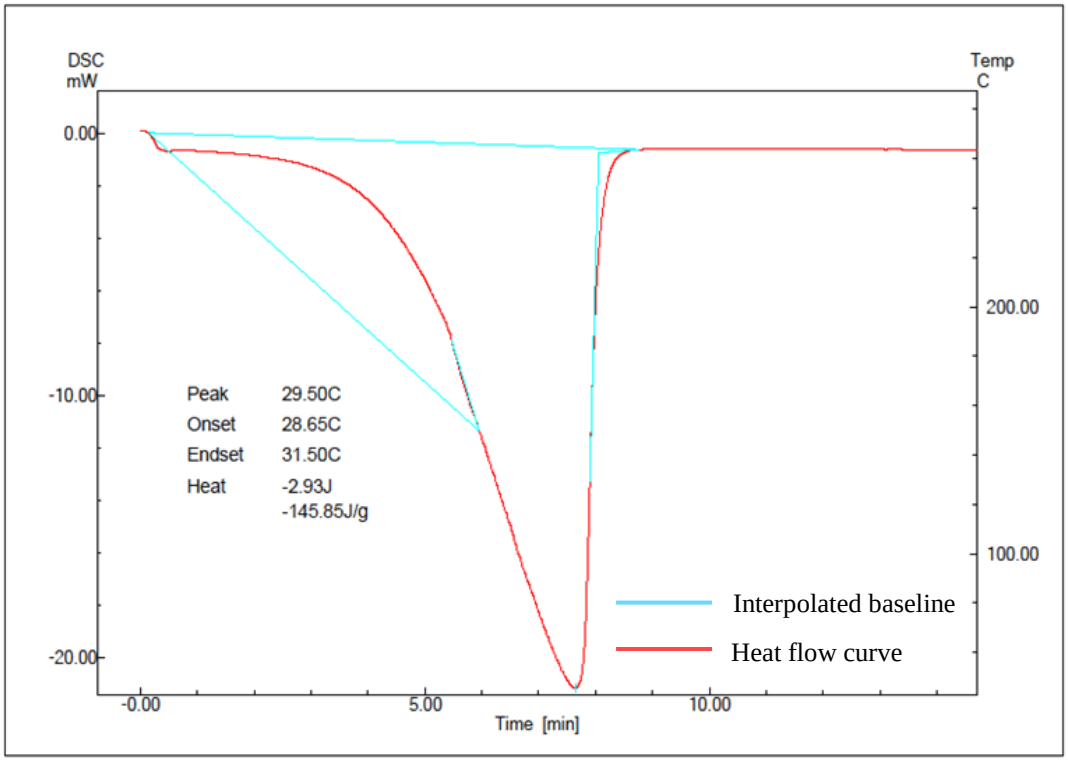

Figure 5.18: DSC analysis of GNPs Sur1 PCM

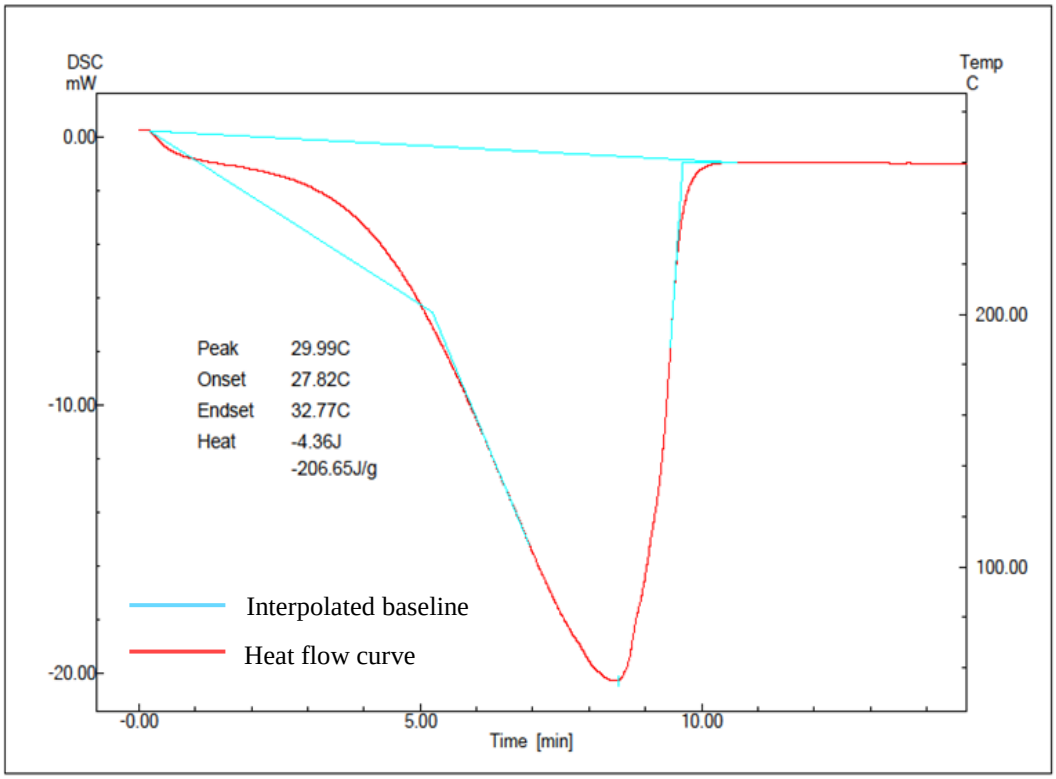

Figure 5.19: DSC analysis of GNPs Sur2 PCM

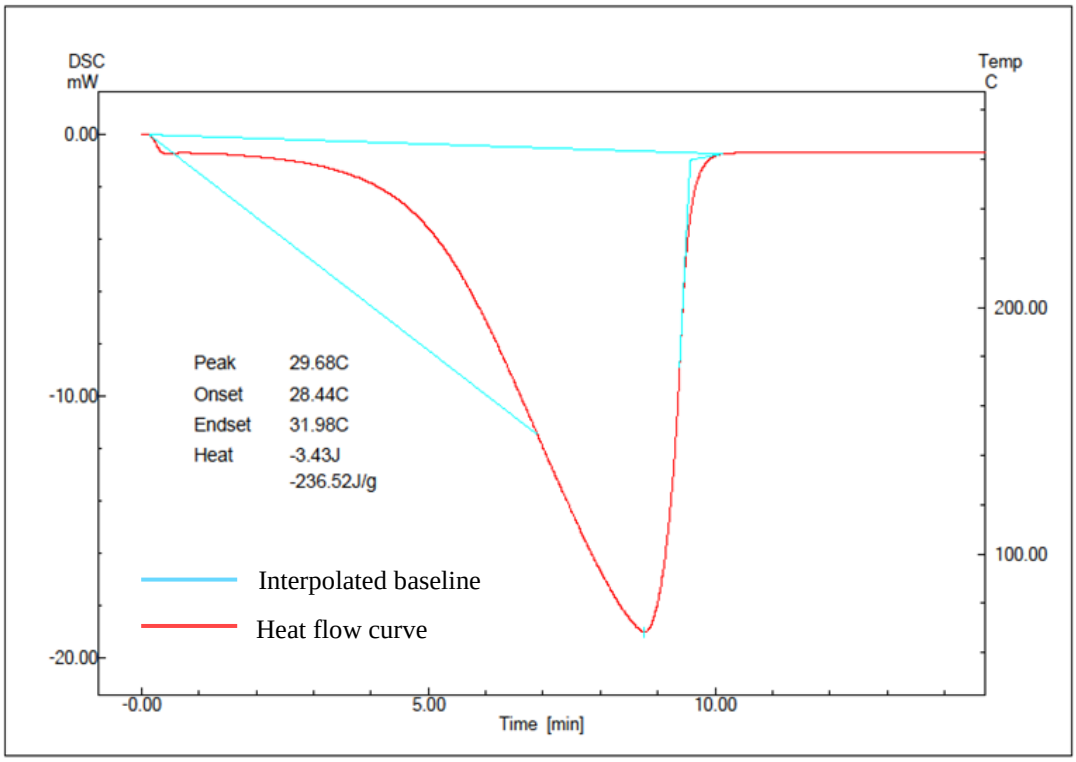

Figure 5.20: DSC analysis of GNPs Sur3 PCM

5.7. The Thermal Performance of Bio-based PCM with GnPs Integrated into a Heat Sink

Figures 5.21, 5.22, and 5.23 represent the varying transient thermal responses of the heater when different surfactants of 1%, 3%, and 5% mass fraction integrated within the GnPs Nano-PCM are used as a heat sink. The current experiment considered four types of PCM based heat sinks that are Pure PCM, NanoPCM-SDBS, NanoPCM-SDS, and NanoPCM-SSL. Here, it is important to recall that the ultimate goal is to establish the best surfactant for the NanoPCM that can augment the thermal performance of the heat sink. As outlined earlier, for this experiment the concentration of GnPs and surfactants within the bio based PCM was fixed at 1%, 3%, and 5% mass fraction (one-to-one ratio) and the transient response was observed. As a result, the effects of surfactant and GnPs concentration on thermal performance is apparent. Furthermore, the thermal response of the heater in the absence of a heat sink was also plotted thereby serving as a control. By running the experiment for a fixed amount of time, approximately 900 seconds in this case, it is possible to satisfactorily compare the thermal performance of each heat sink. This is done by evaluating the final temperature of the heater after the fixed period has been reached. A lower final temperature is indicative of better thermal cooling characteristics since it shows that more heat was absorbed by the heat sink in a given period.

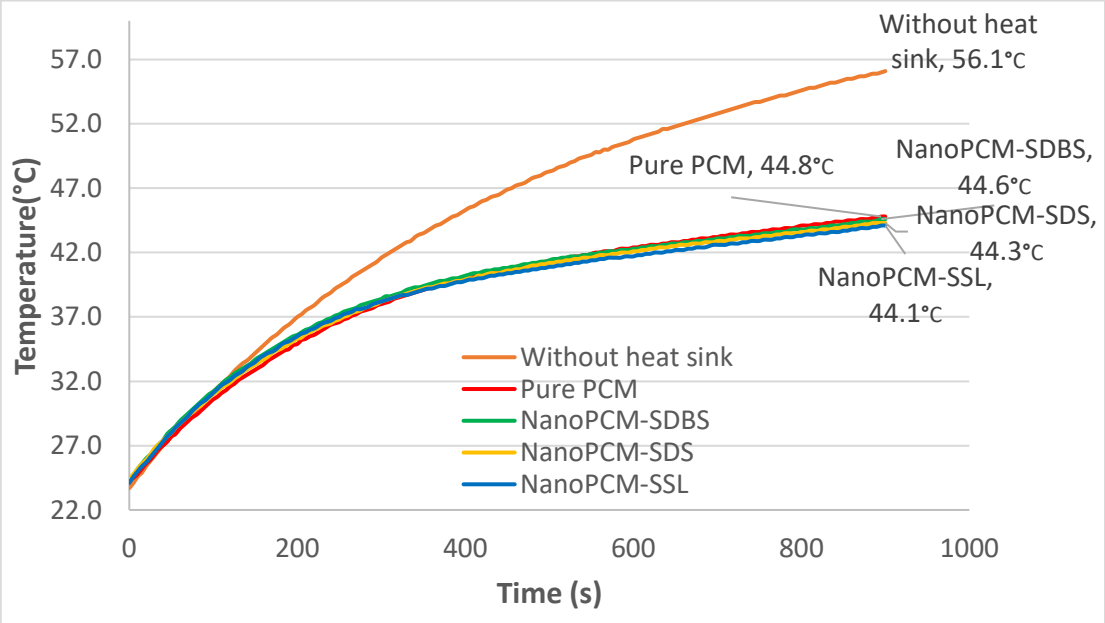

Figure 5.21: Transient thermal responses of the heater at 10 W power using GnPs-PCM with different surfactants of 1% mass fraction of GnPs-surfactant mixture (1:1) as a heat sink

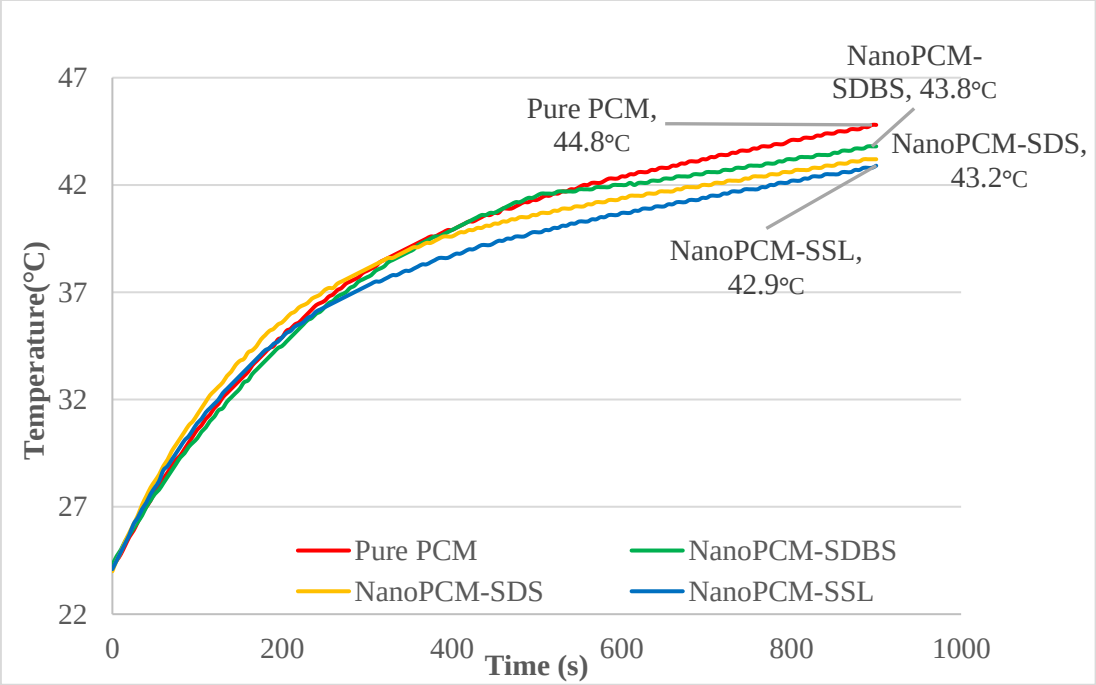

Figure 5.22: Transient thermal responses of the heater at 10 W power using GnPs-PCM with different surfactants of 3% mass fraction of GnPs-surfactant mixture (1:1) as a heat sink

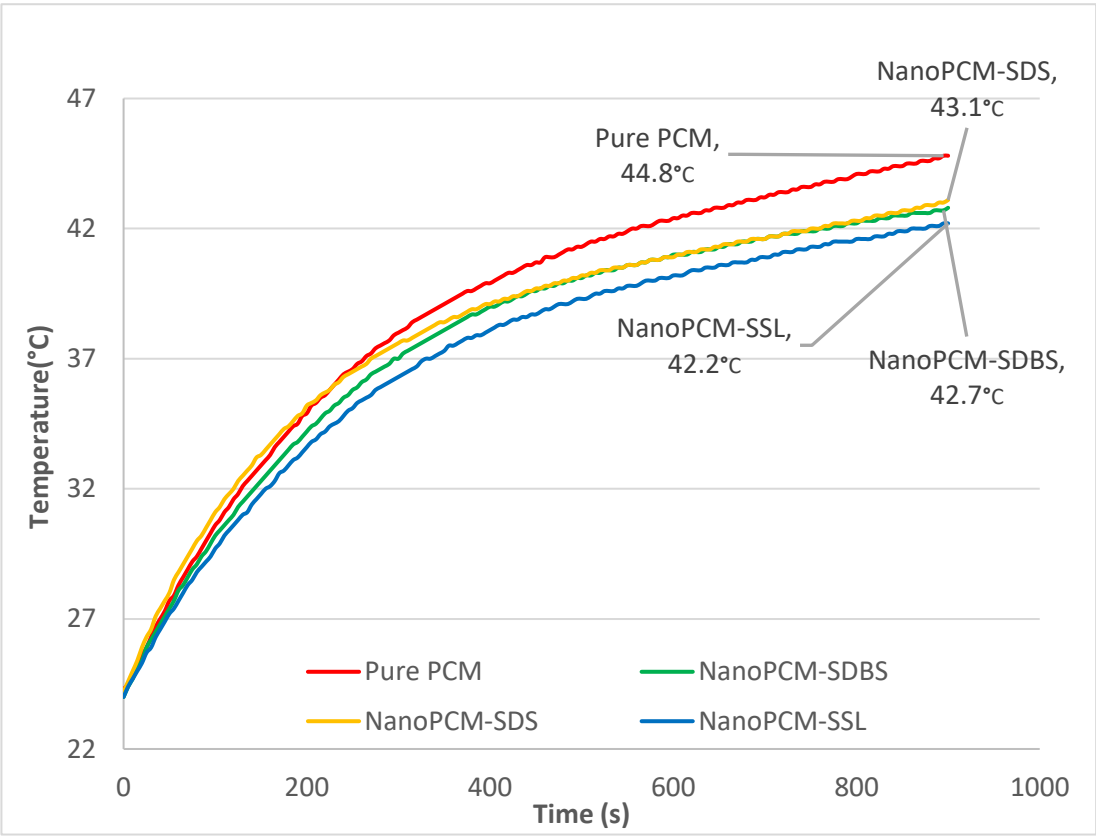

Figure 5.23: Transient thermal responses of the heater at 10 W power using GnPs-PCM with different surfactants of 5% mass fraction of GnPs-surfactant mixture (1:1) as a heat sink

Firstly, the results clearly justify the use of bio-based PCM as a heat sink. since at the end of the 900 second time frame, all four heat sinks recorded a much smaller temperature of at least 44.8 ℃ when compared to the 56.1℃ for the heater without the heat sink. Secondly, it can also be inferred that adding NanoPCM with surfactants improved the thermal performance of the PCM heat sink. This is because all three NanoPCMs, regardless of the type of surfactant used, recorded a lower temperature than the Pure PCM. Comparing the four heat sinks amongst each other, it is easy to identify that that the SSL integrated NanoPCM showed the best heat transfer characteristics since it had the lowest final temperature among the other surfactants for different mass fractions. However, as seen in Figure 5.23, NanoPCM-SSL at 5% mass fraction exhibits the lowest overall temperature at 42.2 ℃ at the end of the 900-second period. Thus, it is important to notice the effect of adding different mass fractions of the GnPs-surfactant mixture that is added at 1:1 ratio. Figures 5.24, 5.25, and 5.26 illustrate how the temperature of the NanoPCM mixed with SDS, SDBS and SSL all decrease with increasing mass fractions at the end of the allocated time.

The time it takes for the hot plate to reach a certain temperature is an important parameter in terms of cooling performance. Therefore, an alternative method to evaluate the heat transfer characteristics of each heat sink is to establish a reference temperature and evaluate the time take by the heater to reach this temperature. Figure 5.24 shows a magnified section of the transient thermal responses of the heater for 1% mass fraction of GnPs where a horizontal line is plotted at the reference temperature of 43℃. Vertical lines extending from each heat sink plot intersect the time-axis to highlight the time taken for each heat sink to reach 43 ℃. A longer time taken is indicative of better cooling performance since it shows that the heat sink cooled the heater at a higher rate and therefore the heater took longer to reach the reference temperature.

The results show re-confirm that NanoPCM with surfactants has a better cooling performance when compared to Pure PCM. This is because the time taken to reach 43 ℃ for all NanoPCM with surfactants was up to 85 seconds more than the time taken by the PurePCM. This indicates a positive percentage difference in time taken to reach 43℃ by up to nearly 12%. In addition, the results also re-affirm that SSL integrated NanoPCM showed the best cooling performance when compared with SDBS or SDS based NanoPCM heat sinks. This is seen since the SSL NanoPCM took 20 seconds

longer than the SDS NanoPCM and up to 65 seconds longer than the SDBS NanoPCM to reach the reference temperature of 43 ℃. This shows that the SSL surfactant exhibited a positive percentage improvement in the time taken to reach 43 ℃ by up to nearly 9% when compared to other surfactants.

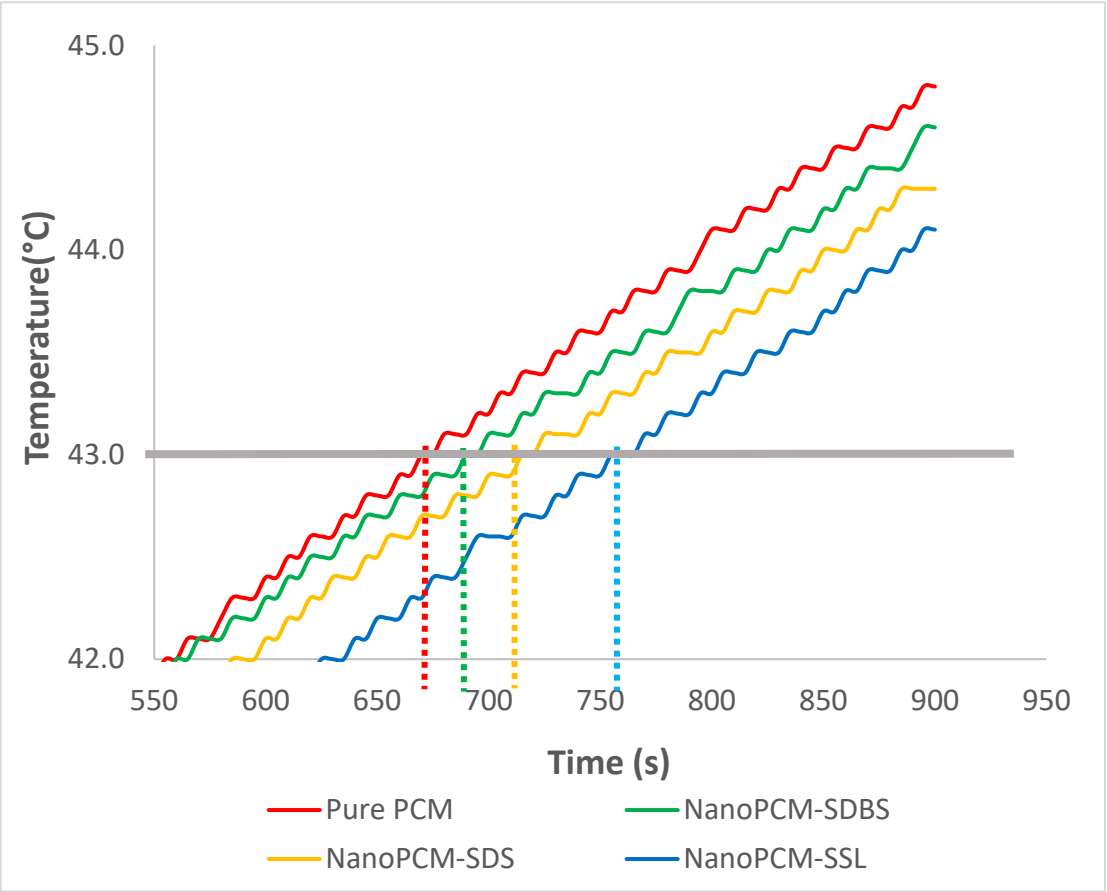

Figure 5.24: Variation of the reach times to 43°C using GnPs-PCM with different surfactants as a heat sink for 1% mass fraction of GnPs-surfactant mixture (1:1)

The plot in Figure 5.25 summarizes the results and displays the effect of 1%, 3% and 5% mass fraction on the time required to reach the reference temperature of 43 ℃. NanoPCM-SSL with a 5% GnPs-surfactant mixture illustrates the largest time to reach the reference temperature at 1015 seconds while pure PCM displays the shortest time at 670 seconds. Therefore, the time required to reach the reference temperature increases for increasing mass fractions as NanoPCM-SDBS at 1% reaches the reference after 695 seconds, then after 770 seconds for 3%, and finally 935 seconds for 5%, which is the greatest time. NanoPCM-SDS and NanoPCM-SSL follow a similar trend where the time constantly rises with increasing mass fractions, which clearly portrays the relation between transient time and the mass fraction of the GnPs-surfactant mixture.

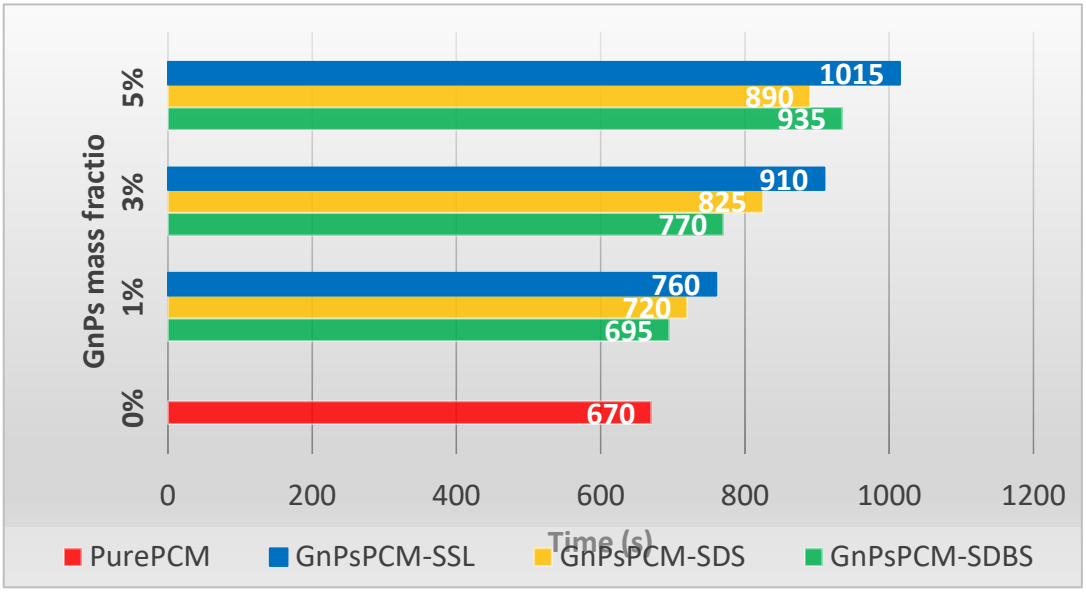

Figure 5.25: Chart showing time taken for each heat sink to reach reference temperature

5.8. Heat Transfer Analysis of PCM Based Heat sink

In this section, the heat transfer analysis is done by calculating the rate of heat absorbed by PCM, Aluminum container and natural convection. Compared to conduction and convection, the heat transfer by radiation is very small due to the limited temperature difference, and therefore it can be neglected.

5.8.1. The rate of heat absorbed by PCM: The rate of heat absorbed by PCM is equal to the summation of the sensible heat of PCM (solid medium), the latent heat of PCM (liquid medium), and the sensible heat of PCM (liquid medium) divided by the total time.

$$\dot{Q}_{pcm} = \frac{m_{pcm}c_{p,s}\,\Delta T + m_{pcm}L + m_{pcm}\,c_{p,l}\,\Delta T}{\Delta t} \qquad (12)$$

Where m_{pcm} is the mass of PCM (g), ΔT is the change in temperature, and Δt is the change in time.

5.8.2 The rate of heat absorbed by Aluminum container: The rate of heat absorbed by PCM is equal to sensible heat of Aluminum.

$$\dot{Q}_{Al} = m_{Al}c_{p,Al}\,\Delta T \qquad (13)$$

5.8.3. The rate of heat transfer by natural convection: To calculate the rate of heat transfer by natural convection($\dot{Q}_{conv}$), equation (14) describing Newton's law of cooling, as noted below, was used:

$$\dot{Q}_{conv} = h\, A_s(T_s - T_\infty) \tag{14}$$

Where A_s is the heat transfer surface area (m^2), T_s is the temperature of the surface (°C), and T_∞ is the temperature of the surrounding air (°C).

Since the rate of heat transfer is the product of heat convection coefficient, the surface area of heat transfer space, and difference between the surface temperature and the ambient space temperature. The ambient space temperature was taken to be 24 ℃.

The heat transfer convection coefficient (h), in equation (14), is calculated as shown below in equation (15) [39]:

$$h = \frac{k}{L_c} Nu \tag{15}$$

Where k is the thermal conductivity (w/m. K), and L_c is the characteristic length of the geometry (m).

The value of the convection heat transfer coefficient (h) depends on every parameter linked to convection. A dimensionless convection heat transfer coefficient that is directly proportional to the heat transfer through convection is called Nusselt number. The natural convection Nusselt number for the horizontal plate with heat transfer taking place in upward direction is found using the below equation [39]:

$$Nu = 0.27 Ra_L^{\frac{1}{4}} \tag{16}$$

The natural convection Nusselt number for vertical plate is found using the follow equation [39]:

$$Nu = \left\{ 0.825 + \frac{0.387 Ra_L^{\frac{1}{6}}}{\left[1+(0.492/Pr)^{9/16}\right]^{8/27}} \right\}^2 \tag{17}$$

Rayleigh number [39]:

$$Ra_L = \frac{g\beta\,(T_s - T_\infty) {L_c}^3}{\upsilon^2}\, Pr \tag{18}$$

The ratio of the product of the thermal and momentum diffusivities and buoyancy forces is called Rayleigh number (Ra). Rayleigh number is also obtained through the product of Prandtl number and Grashof number. Using equations (12), (13),

(14), (15), (16), (17) and (18), the results are summarized in Figure 5.26 which graphically describes the segments of the rate of heat absorbed by different components in the control system, including pure PCM.

As expected, not all of the heat is completely transferred to the PCM. For a fixed period, pure PCM absorbs 60% of heat while a very minute fraction of the heat, amounting to 8% of the heat, is absorbed by the container in which the PCM is contained. Notably, the convective conditions on top of the bio-PCM are responsible for 4% of the total transmission of heat for a fixed period of time.

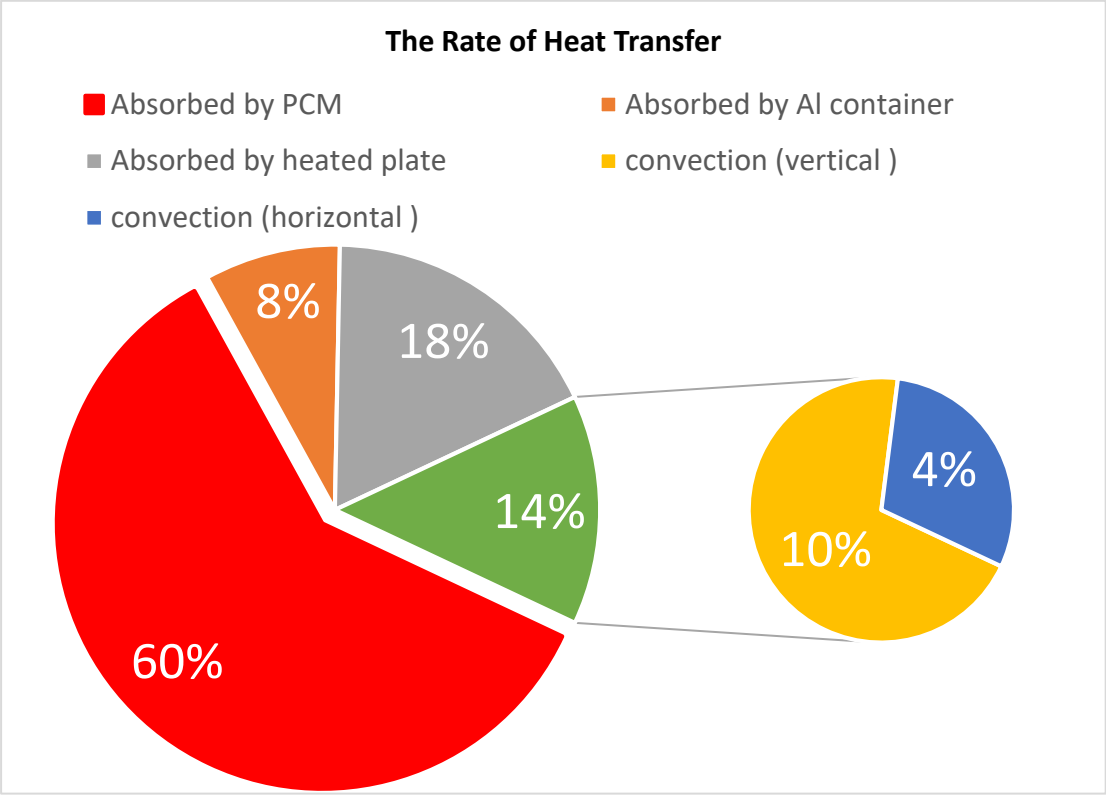

Figure 5.26: Pie chart showing Heat Transfer Analysis of PCM Based Heat sink

5.9. Thermal Conductivity of Graphite/Bio-based PCM Composites

The current experiment considered four types of PCM based heat sinks, that are; Pure PCM, GraPCM-SDBS, GraPCM-SDS, and GraPCM-SSL. It must be noted that the case of GraPCM-SSL proved to be highly unstable in all combinations of the concentration ratio's studied, leading to an outlier data. Hence, this data was discarded and not documented.

Here, it is important to recall that the ultimate goal is to establish the best surfactant for the NanoPCM that can augment the thermal performance of the heat sink.

To quantify thermal performance, thermal qualities such as thermal conductivity and temperature response over time were studied for various combinations of heat sink fluids including pure PCM which served as a control sample for reference.

Based on the procedure prescribed, data was obtained from experiments conducted for graphite to surfactant ratios of 1:3, 1:4 and 1:5, and varying mass fraction of graphite of 1%, 3% and 5% within the mixture. It must be noted that the case of varying mass fractions are documented only for mixtures with concentration ratio of 1:3 since the temperature response for the mixtures at 1:4 and 1:5 concentration ratio were undesirable due to high values. Hence, mass fraction variations only for the case of 1:3 concentration ratio are plotted and explained, as these present the best-case scenario in terms of thermal performance values.

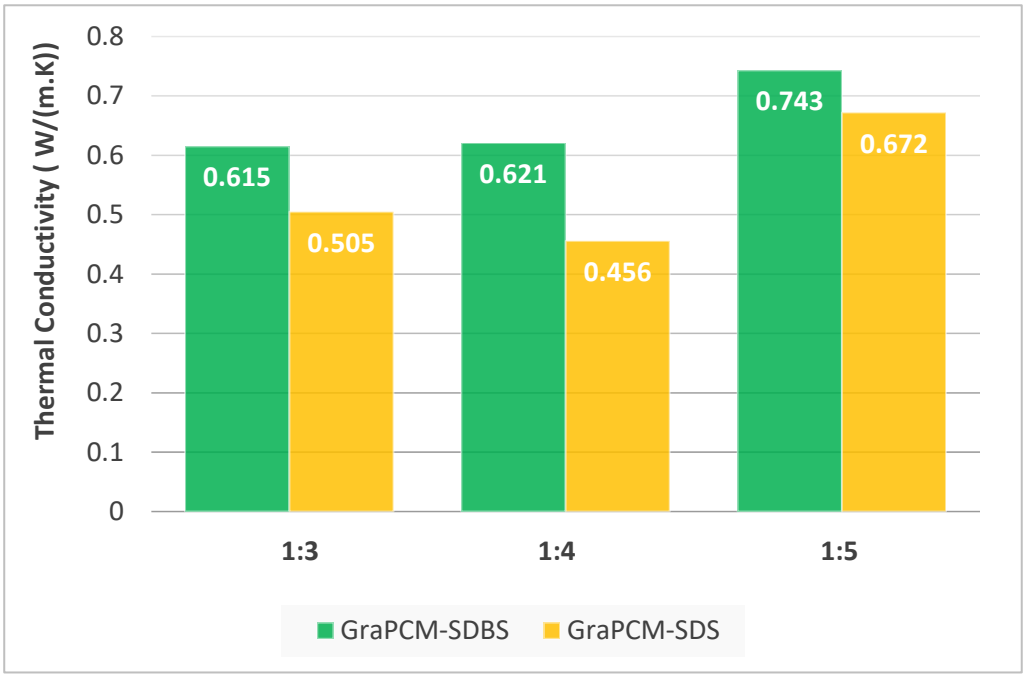

Figure 5.27: Thermal Conductivity of Different PCM Mixtures and Varying Graphite to Surfactant Ratio at 1% Mass Fraction of Graphite

The thermal conductivity of the pure bio-based PCM infused with SDBS and SDS surfactants are shown in Figures 5.27and 5.28. While Figure 5.27 portrays data for different graphite to surfactant ratio at 1% mass fraction of graphite, Figure 5.28 displays data for different mass fractions of graphite within the mixture at a fixed graphite to surfactant concentration ratio of 1:3.

From Figure 5.27, it is evident that thermal conductivity in the case of SDBS infused Graphite PCM outperforms thermal conductivity of Graphite PCM with SDS

surfactant. The highest thermal conductivity for GraPCM-SDBS and GraPCM-SDS is noted in the case of 1:5 graphite to surfactant ratio. It is also noted that, with increment in concentration of surfactant within the mixture, the thermal conductivity of GraPCM-SDBS increases. However, this trend is not observed in GraPCM-SDS as the thermal conductivity of GraPCM-SDS at 1:4 concentration ratio is lower than the case of 1:3. GraPCM-SDS does not have a large increment in thermal conductivity with an increment of surfactant concentration from three-fold to four-fold as the thermal conductivity only increments by 0.9%. However, the effect is well pronounced in the case of increment from 1:4 to 1:5, as thermal conductivity increases by 16%.

From Figure 5.28, amongst other combinations, GraPCM-SDBS displays the highest thermal conductivity at 5% mass fraction of graphite for 1:3 graphite to surfactant ratio. GraPCM-SDS has the highest thermal conductivity at 5% mass fraction of graphite when compared against its thermal conductivity values at different graphite mass fractions. GraPCM-SDS displays a trend of incrementing thermal conductivity with increase in graphite mass fraction at 1:3 concertation ratio. However, this trend is not observed in GraPCM-SDBS as the thermal conductivity of GraPCM-SDBS at 3% concentration ratio is lower than the case of 1%.

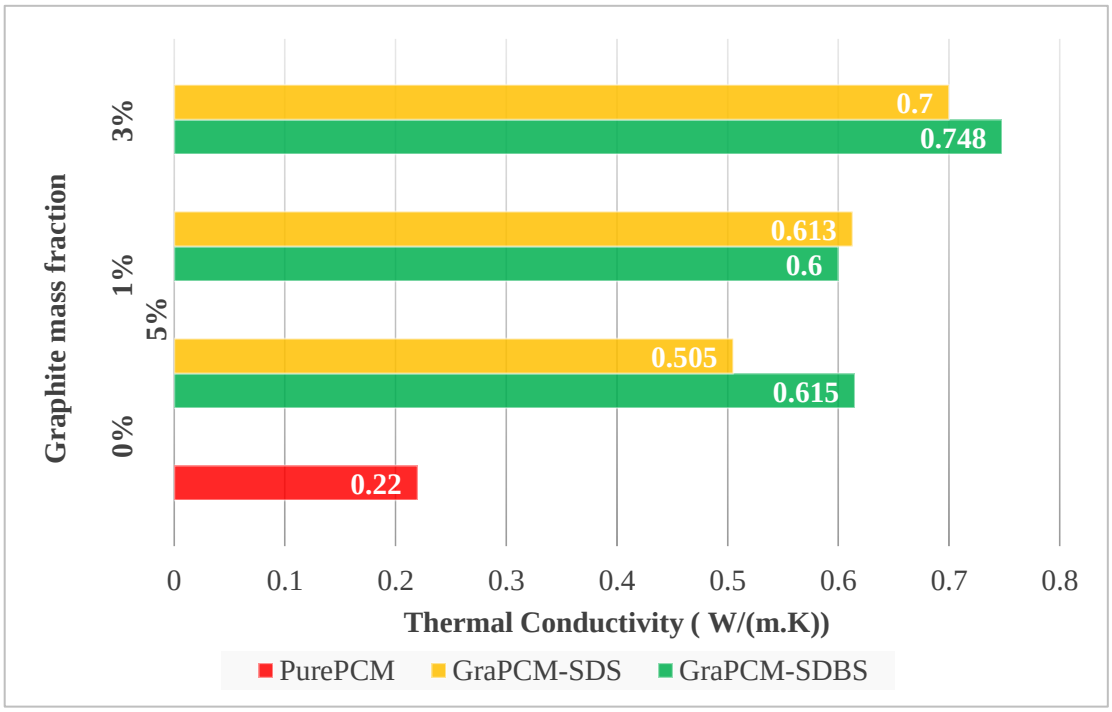

Figure 5.28: Thermal Conductivity of Differing PCM Mixtures and Varying Mass Fraction of Graphite at 1:3 Graphite to Surfactant Ratio

5.10. The Thermal Performance of Bio-Based PCM with Graphite Integrated into a Heat Sink

Another characteristic index of thermal performance is temperature response over time. By running the experiment for a fixed amount of time, approximately 900 seconds in this case, it is possible to satisfactorily compare the thermal performance of each heat sink. This is done by evaluating the final temperature of the heater after the fixed time frame has been reached. A lower final temperature is indicative of better thermal cooling characteristics since it shows that more heat was absorbed by the heat sink in a given period.

Figures 5.29, 5.30 and 5.31 portray the transient thermal responses of the heater when GraPCM-SDS and GraPCM-SDBS are mixed with 1:3 graphite to surfactant ratio at 1% mass fraction of graphite. Figures 5.32 and 5.33, chart the data for the mixtures at mass fractions of 3% and 5%, respectively, at 1:3 graphite to surfactant ratio.

From Figure 5.29 in the case of 1:3 concentration ratio at 1% mass fraction of Graphite, the final temperature GraPCM-SDS and GraPCM-SDBS is 44.2 °C and 43.8 °C, respectively. This justifies the use of surfactant at the given level of mixture composition, as the final temperatures of both mixtures are lesser than that of pure PCM.

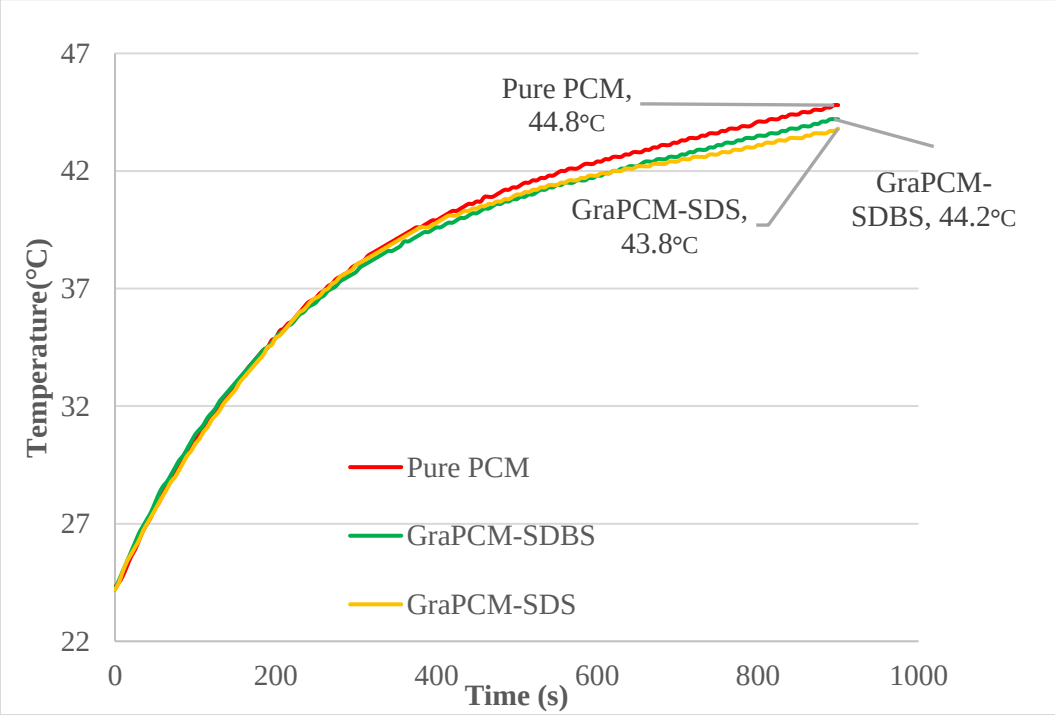

Figure 5.29: Temperature Response against Time of PCM Mixtures at Mass Fraction of Graphite of 1% and 1:3 Graphite to Surfactant Ratio

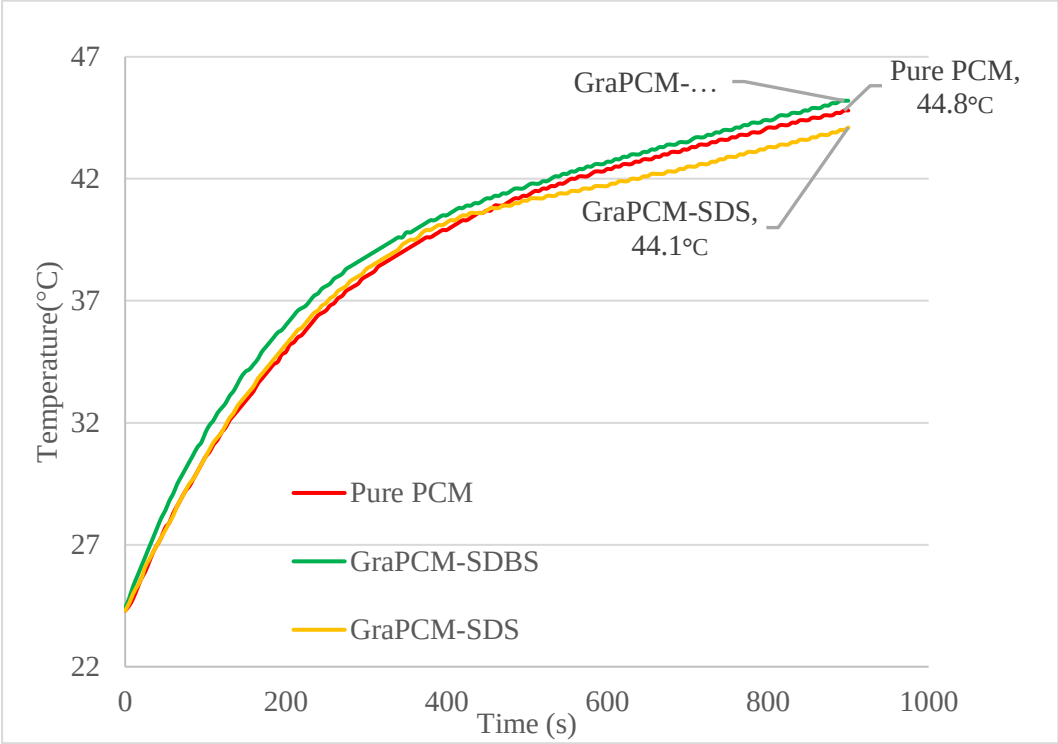

Figure 5.30: Temperature Response against Time of PCM Mixtures at Mass Fraction of Graphite of 1% and 1:4 Graphite to Surfactant Ratio

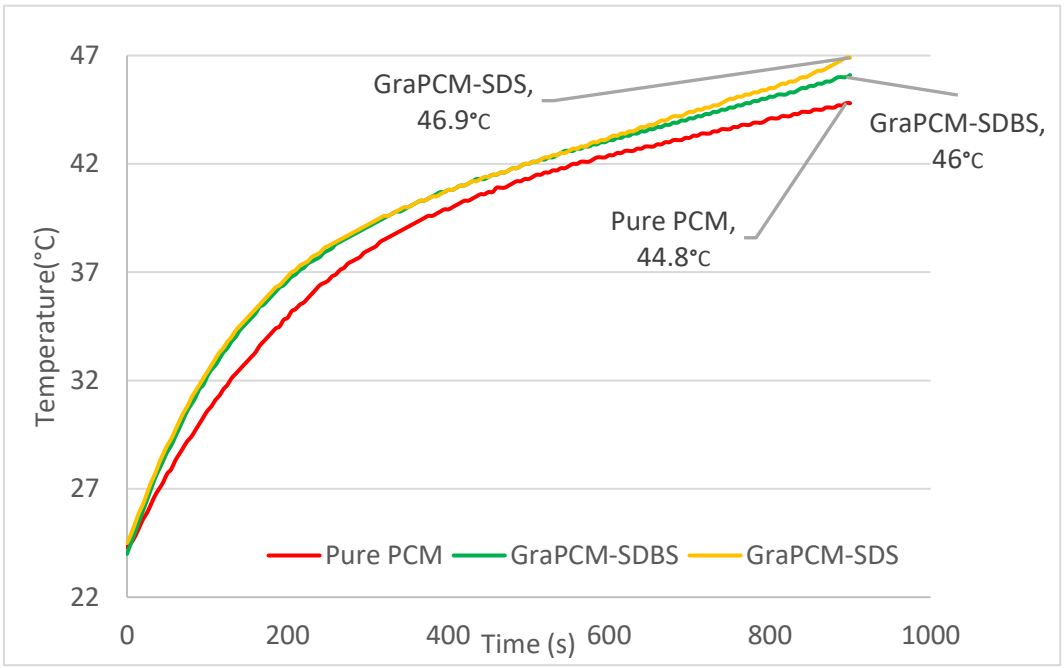

Figure 5.31: Temperature Response against Time of PCM Mixtures at Mass Fraction of Graphite of 1% and 1:5 Graphite to Surfactant Ratio

From Figures 5.30 and 5.31, the use of GraPCM-SDBS is not recommended in the case of concentration ratios of 1:4 and 1:5 at 1% mass fraction of graphite as the

final temperature is higher than pure PCM. This is due to final temperatures of GraPCM-SDBS being 45.2°C and 46°C at 1:4 and 1:5 concentration ratio's, respectively. GraPCM-SDS also has higher final temperature than that of pure PCM in the case of 1:5 concentration ratio; however, it is lower than that of pure PCM in the case of 1:4 concentration ratio with a final temperature of 44.1 °C.

Concentration ratios of 1:4 and 1:5 at different mass fractions of graphite yielded, if not similar, even poor transient thermal response with higher final temperatures at the end of 900 seconds.

However, the case of 1:3 concentration ratio yielded strong thermal performance data in terms of temperature response at 1%, 3% and 5% graphite mass fraction. This is evident from the Figures 5.29, 5.32 and 5.33. Figure 5.32 displays the case of 3% mass fraction of graphite infused in 1:3 graphite to surfactant concentration ratio. This case yields better further reduction of the recorded final temperature of GraPCM-SDS and GraPCM-SDBS when compared to the case of 1% graphite mass fraction in 1:3 concentration ratio. The final temperature of GraPCM-SDBS after 900 seconds of heating at 10W was found to be 43.8°C, while the final temperature of GraPCM-SDS was 43.5°C.

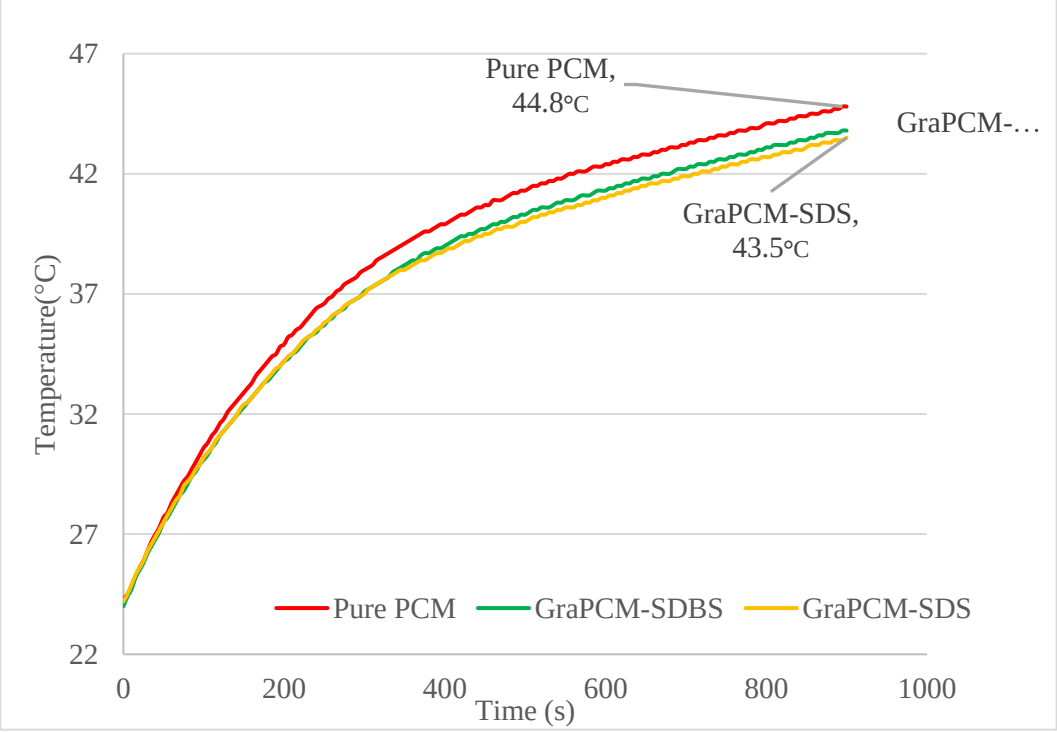

Figure 5.32: Temperature Response against Time of PCM Mixtures at Mass Fraction of Graphite of 3% and 1:3 Graphite to Surfactant Ratio

On increment of the graphite mass fraction to 5% at the same concentration ratio of 1:3, further reduction in final temperature was noticed. From Figure 5.33, the final temperature of GraPCM-SDBS was 43.4 °C and final temperature of GraPCM-SDS remained unaffected at 43.5.

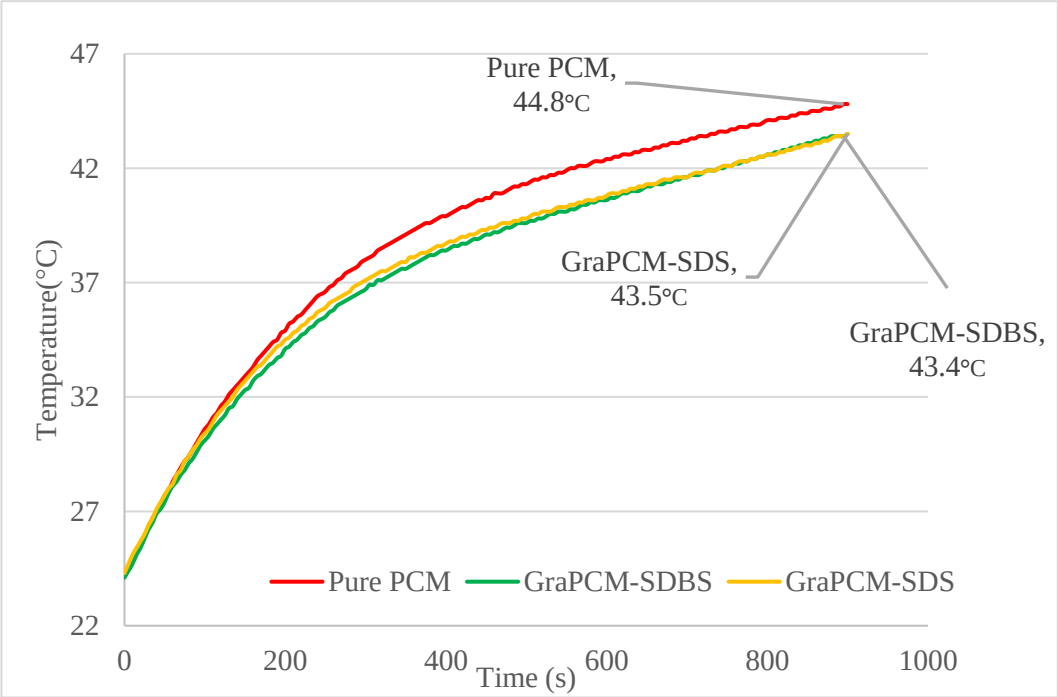

Figure 5.33: Temperature Response against Time of PCM Mixtures at Mass Fraction of Graphite of 5% and 1:3 Graphite to Surfactant Ratio

The time taken to reach the reference temperature of 43 °C for the pure bio-based PCM infused with SDBS and SDS surfactants are shown in Figures 5.34 and 5.35. While Figure 5.34 portrays time data for different graphite to surfactant ratio at 1% mass fraction of graphite, Figure 5.35 displays time data for different mass fractions of graphite within the mixture at a fixed graphite to surfactant concentration ratio of 1:3.

From Figure 5.34, it is evident that time taken to reach reference temperature in the case of SDBS infused Graphite PCM outperforms the same parameter of Graphite PCM with SDS surfactant. The longest delay in time for GraPCM-SDBS and GraPCM-SDS is noted in the case of 1:3 graphite to surfactant ratio. In this case, the time taken by GraPCM-SDBS was 740 seconds while the time taken by GraPCM-SDS was 785 seconds. Hence, GraPCM-SDS shows the highest resistance, thus, absorbing more heat within the same period of time. It is also noted that, with increment in concentration of

surfactant within the mixture, both mixtures show lesser resistance to reach the final temperature and do so with lesser delay.

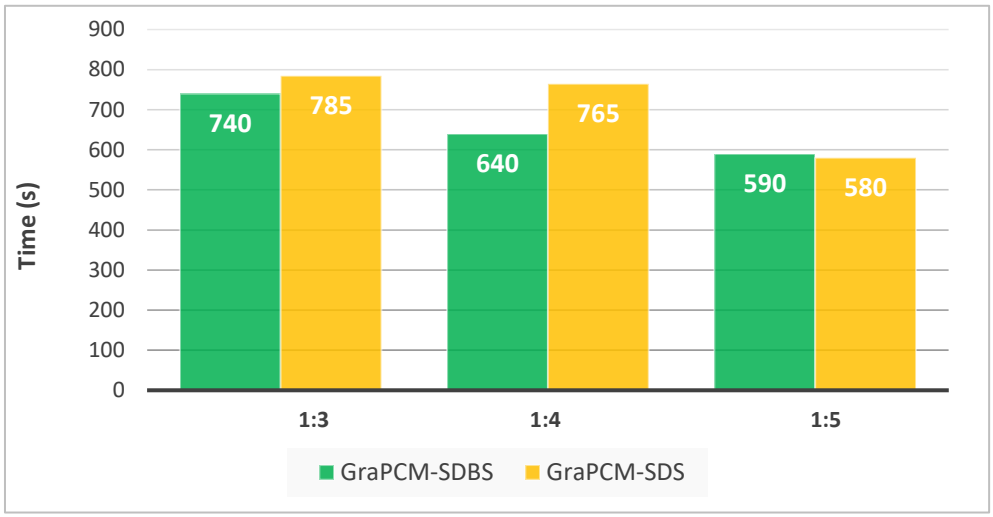

Figure 5.34: Time Taken to Reach 43°C of Different PCM Mixtures at Varying Concentration of Graphite to Surfactant Ratio at Mass Fraction of Graphite of 1%

From Figure 5.35, amongst other combinations, GraPCM-SDS displays longest time taken at 5% mass fraction of graphite for 1:3 graphite to surfactant ratio. GraPCM-SDBS takes the longest time to reach the reference temperature at 5% mass fraction of graphite when compared against time taken to reach the same temperature at different graphite mass fractions. GraPCM-SDBS and GraPCM-SDS displays a trend of incrementing thermal conductivity with increase in graphite mass fraction at 1:3 concentration ratio.

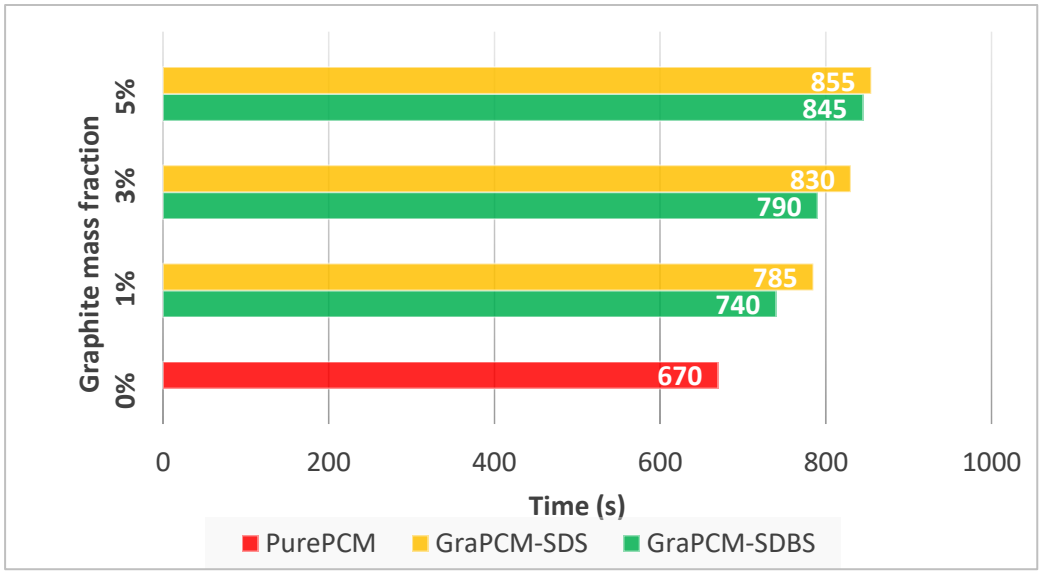

Figure 5.35: Time Taken to Reach 43°C of Different PCM Mixtures at Mass Fraction of Graphite of 5% and 1:3 Graphite to Surfactant Ratio

5.11. The Comparison between Experimental and Numerical Results

The results of the experiment and the numerical analysis of the plate temperature when using PCM as a heat sink are plotted in Figure 5.36. Experimental and numerical results agreed strongly when pure PCM was used as a heat sink.

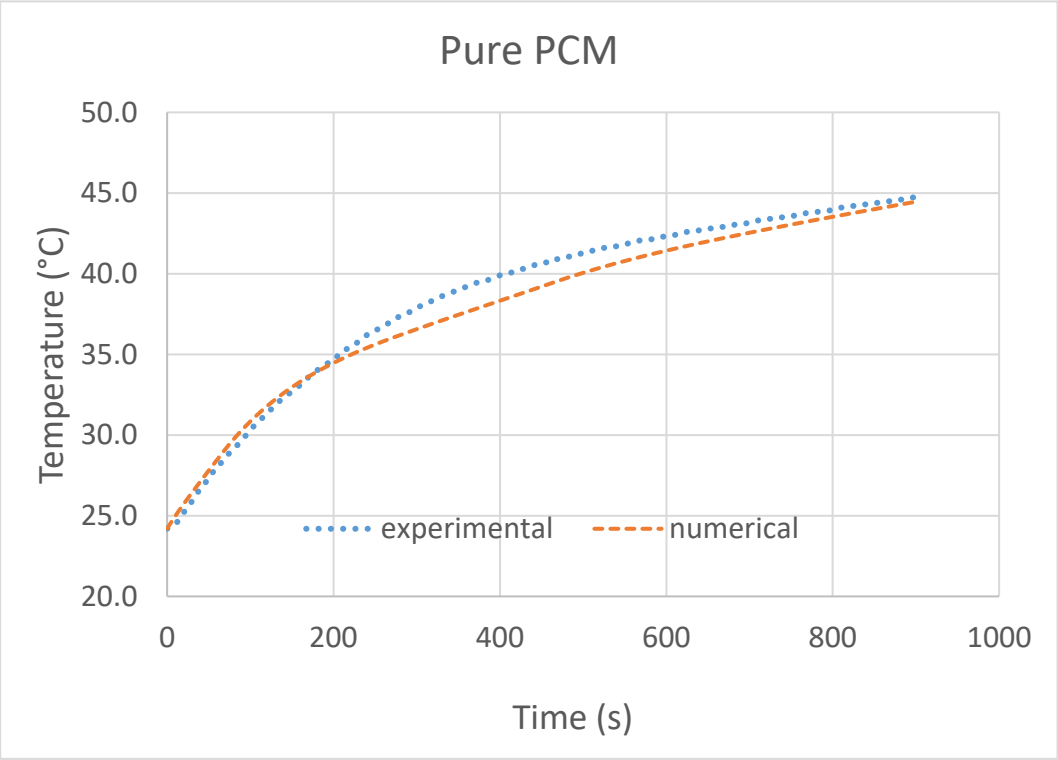

Figure 5.36: Comparison of numerical and experimental results of the plate temperature over time using PCM as a heat sink

Chapter 6. Conclusion and Recommendations

6.1. Summary

Vapor compression refrigeration system is one of the most promising cooling techniques for electronics cooling in general and for high heat dissipation electronics cooling in particular. A small Vapor Compression Refrigeration (VCR) system integrated with PCM is proposed to cope with the increasing demand for smaller and powerful electronics. The system is designed for laptop cooling with a cooling capacity of 100 W and the dimension of the system is 38 × 30× 15 cm. While modeling the performance of the system, it is found that R134a has the best performance among the others.

6.2. Conclusion

Thermal data such as latent heat, thermal conductivity, and temperature response for the surfactant induced GnPs-PCM, and Gra-PCM were compared with pure PCM. Although all the surfactants induced PCM-GnPs closely matched each other, NanoPCM-SDS had the highest thermal conductivity in solid state, reporting an increase in thermal conductivity by of 368%, therefore, largely outperforming pure PCM. On average, the thermal conductivity of GnPs-PCM was 4.1 times higher than Pure PCM, when it was mixed with different Surfactants, while the thermal conductivity of Gra-PCM was 3.3 times higher than Pure PCM. The results indicate a strong correlation between the surfactant and thermal conductivity enhancement.

The time it takes for the hot plate to reach a certain temperature is an important parameter in terms of cooling performance. SSL Surfactant took the longest time to reach the reference temperature, when it was mixed with GnPs-PCM, reporting an increase in time difference by 51% when compared to Pure PC.

SSL-GnPs-PCM is the best option as it reported the longest time to reach the reference temperature, providing a 345-sec delay compared to the Pure PCM, thereby outlining its potency as a more effective heat sink when compared to Pure PCM as well as the other surfactants. A good agreement between experimental and numerical result had been achieved, when the Pure PCM was used as a heat sink.

The results obtained agreed with literature as an addition of surfactants and GnPs or graphite to the PCM enhanced the thermal conductivity and delayed the time response to reach the reference temperature. This study re-affirms the importance of PCMs when cooling performance is considered. Furthermore, satisfactory conclusions

have been with regard to the best possible combination of surfactants with GnPs-PCM. As a result, such research can be taken forward and be implemented in the cooling of electronic devices using the surfactant induced GnPs-PCM heat sink.

The maximum CPU temperature was found to be 67 °C, when the laptop cooler was used, while it was 78 °C without using the cooler. Noticeably, when the cooler was used that helped in reducing the temperature of CPU by 11 degrees (14.1%), the temperature of the CPU was more suppressed.

6.3. Recommendations

Since direct contact heat transfer is better than indirect contact heat transfer, it is recommended that laptops should have an opening at the bottom side to allow for direct contact between PCM and the heat source (CPU).

References

[1] S. Fok, W. Shen, and F. Tan, “Cooling of portable hand-held electronic devices using phase change materials in finned heat sinks,” *International Journal of Thermal Sciences*, vol. 49, no. 1, pp. 109–117, 2010.

[2] L. T. Yeh, “Review of Heat Transfer Technologies in Electronic Equipment,” *Journal of Electronic Packaging*, vol. 117, no. 4, pp. 333–339, 1995.

[3] W. G. Alshaer, S. A. Nada, M. A. Rady, E. P. Del Barrio, and A. Sommier, "Thermal management of electronic devices using carbon foam and PCM/nano-composite," *International Journal of Thermal Sciences,* vol. 89, pp. 79-86, 2015.

[4] T. T. Mattila, J. Li, and J. K. Kivilahti, "On the effects of temperature on the drop reliability of electronic component boards," *Microelectronics Reliability,* vol. 52, no. 1, pp. 165-179, 2012.

[5] E. Sevinchan, I. Dincer, and H. Lang, "A review on thermal management methods for robots," *Applied Thermal Engineering,* vol. 140, pp. 799-813, 2018.

[6] C. W. Chan, E. Siqueiros, J. Ling-Chin, M. Royapoor, and A. P. Roskilly, "Heat utilisation technologies: A critical review of heat pipes," *Renewable and Sustainable Energy Reviews,* vol. 50, pp. 615-627, 2015.

[7] C. J. M. Lasance and R. E. Simons, "Advances in high-performance cooling for electronics." *Electronics Cooling*, vol. 11, no. 4, pp. 22-39,2015.

[8] A. Mota-Babiloni, "Analysis of low Global Warming Potential fluoride working fluids in vapour compression systems. Experimental evaluation of commercial refrigeration alternatives. " PhD dissertation, Polytechnic University of Valencia, Spain, 2016.

[9] A. R. M. Siddique, S. Mahmud, and B. V. Heyst, "A comprehensive review on a passive (phase change materials) and an active (thermoelectric cooler) battery thermal management system and their limitations," *Journal of Power Sources,* vol. 401, pp. 224-237, 2018.

[10] Y.-H. Wang and Y.-T. Yang, "Three-dimensional transient cooling simulations of a portable electronic device using PCM (phase change materials) in multi-fin heat sink," *Energy*, vol. 36, no. 8, pp. 5214-5224, 2011.

[11] H. Mehling and L. F. Cabeza, *Heat and cold storage with PCM an up to date introduction into basics and applications*. Berlin: Springer, 2010, pp. 11–55.

[12] B. E. Jebasingh, “Thermal Conductivity on Ternary Eutectic Fatty Acid as Phase Change Material (PCM) by Various Treated Exfoliated Graphite Nanoplatelets (xGnP),” *Frontiers in Materials Processing, Applications, Research and Technology*, pp. 75–84, 2017.

[13] J. Li, D. Liang, K. Guo, R. Wang, and S. Fan, "Formation and dissociation of HFC134a gas hydrate in nano-copper suspension," *Energy Conversion and Management,* vol. 47 ,no. 2, pp. 201-210, 2006.

[14] G. Li, Y. Hwang, and R. Radermacher, "Review of cold storage materials for air conditioning application," *International Journal of Refrigeration,* vol. 35, no. 8, pp. 2053-2077, 2012.

[15] E. M. Alawadhi and C. H. Amon, "PCM thermal control unit for portable electronic devices: experimental and numerical studies," *IEEE Transactions on Components and Packaging Technologies,* vol. 26, no. 1, pp. 116-125, 2003.

[16] A. Hasan, H. Hejase, S. Abdelbaqi, A. Assi, and M. Hamdan, "Comparative Effectiveness of Different Phase Change Materials to Improve Cooling Performance of Heat Sinks for Electronic Devices," *Applied Sciences*, vol. 6, no. 9, p. 226, 2016.

[17] R. Kandasamy, X.-Q. Wang, and A. S. Mujumdar, "Transient cooling of electronics using phase change material (PCM)-based heat sinks," *Applied Thermal Engineering,* vol. 28, no. 8, pp. 1047-1057, 2008.

[18] Y. Tomizawa, K. Sasaki, A. Kuroda, R. Takeda, and Y. Kaito, "Experimental and numerical study on phase change material (PCM (for thermal management of mobile devices," *Applied Thermal Engineering,* vol. 98, pp. 320-329, 2016.

[19] T. Ahmed, M. Bhouri, D. Groulx, and M. A. White, "Passive thermal management of tablet PCs using phase change materials: Continuous operation," *International Journal of Thermal Sciences,* vol. 134, pp. 101-115, 2018.

[20] F. L. Tan and C. P. Tso, "Cooling of mobile electronic devices using phase change materials," *Applied Thermal Engineering,* vol. 24, no. 2, pp. 159-169, 2004.

[21] S. F. Hosseinizadeh, F. L. Tan, and S. M. Moosania, "Experimental and numerical studies on performance of PCM-based heat sink with different configurations of internal fins," *Applied Thermal Engineering,* vol. 31, no. 17, pp. 3827-3838, 2011.

[22] S. K. Sahoo, M. K. Das, and P. Rath, "Hybrid Cooling System for Electronics Equipment During Power Surge Operation," *IEEE Transactions on Components, Packaging and Manufacturing Technology,* vol. 8, no. 3, pp. 416-426, 2018.

[23] S. Motahar and R. Khodabandeh, "An experimental assessment of nanostructured materials embedded in a PCM-based heat sink for transient thermal management of electronic," *Transp Phenom Nano Micro Scales,* vol. 6, no. 2, pp. 96-103, 2018.

[24] R. Mongia, K. Masahiro, E. Distefano, J. Barry, W. Chen, M. Izenson, F. Possamai, A. Zimmermann, and M. Mochizuki, "Small scale refrigeration system for electronics cooling within a notebook computer," *Thermal and Thermomechanical Proceedings 10th Intersociety Conference on Phenomena in Electronics Systems,* 2006, pp. 751-758.

[25] A. A. Nnanna, "Application of refrigeration system in electronics cooling," *Applied Thermal Engineering,* vol. 26, no. 1, pp. 18–27, 2006.

[26] S. Trutassanawin, E. A. Groll, S. V. Garimella, and L. Cremaschi, "Experimental Investigation of a Miniature-Scale Refrigeration System for Electronics Cooling," *IEEE Transactions on Components and Packaging Technologies,* vol ,29 .no. 3, pp. 678-687, 2006.

[27] C. Chang, N. Liang, and S. Chen, "Miniature Vapor Compressor Refrigeration System for Electronic Cooling," *IEEE Transactions on Components and Packaging Technologies,* vol. 33, no. 4, pp. 794-800, 2010.

[28] S. Mancin, C .Zilio, G. Righetti, and L. Rossetto, "Mini Vapor Cycle System for high density electronic cooling applications," *International Journal of Refrigeration*, vol. 36, no. 4, pp. 1191-1202, 2013.

[29] Z. Wu and R. Du, "Design and experimental study of a miniature vapor compression refrigeration system for electronics cooling," *Applied Thermal Engineering*, vol. 31, no. 2, pp. 385-390, 2011.

[30] M. Parlak, K. Sömek, Ü. N. Temel, and K. Yapici, "Experimental investigation of transient thermal response of phase change material embedded by Graphene nanoparticles in energy storage module," in *2016 15th IEEE Intersociety Conference on Thermal and Thermomechanical Phenomena in Electronic Systems (ITherm)*, 2016, pp. 645-651.

[31] M. Mehrali, S. T. Latibari, M. Mehrali, T. M. I. Mahlia, H. S. C. Metselaar, M. S. Naghavi, E. Sadeghinezhad, and A. R. Akhiani, "Preparation and characterization of palmitic acid/graphene nanoplatelets composite with remarkable thermal conductivity as a novel shape-stabilized phase change material," *Applied Thermal Engineering*, vol. 61, no. 2, pp. 633–640, 2013.

[32] U. N. Temel, K. Somek, M. Parlak, and K. Yapici, "Transient thermal response of phase change material embedded with graphene nanoplatelets in an energy storage unit," *Journal of Thermal Analysis and Calorimetry*, vol. 133, no. 2, pp. 907–918, 2018.

[33] Z. Ling, J. Chen, T. Xu, X. Fang, X. Gao, and Z. Zhang, "Thermal conductivity of an organic phase change material/expanded graphite composite across the phase change temperature range and a novel thermal conductivity model," *Energy Conversion and Management*, vol. 102, pp. 202–208, 2015.

[34] F. Wang, J. Liu, X. Fang, and Z. Zhang, "Graphite nanoparticles-dispersed paraffin/water emulsion with enhanced thermal-physical property and photo-thermal performance," *Solar Energy Materials and Solar Cells*, vol. 147, pp. 101–107, 2016.

[35] T. Xu, Q. Chen, G. Huang, Z. Zhang, X. Gao, and S. Lu, "Preparation and thermal energy storage properties of d-Mannitol/expanded graphite composite phase change material," *Solar Energy Materials and Solar Cells*, vol. 155, pp. 141–146, 2016.

[36] S. Zhang, J.-Y. Wu, C.-T. Tse, and J. Niu, "Effective dispersion of multi-wall carbon nano-tubes in hexadecane through physiochemical modification and decrease of supercooling," *Solar Energy Materials and Solar Cells*, vol. 96, pp. 124–130, 2012.

[37] K. Cacua, F. Ordoñez, C. Zapata, B. Herrera, E. Pabón, and R. Buitrago-Sierra, "Surfactant concentration and pH effects on the zeta potential values of alumina nanofluids to inspect stability," *Colloids and Surfaces A: Physicochemical and Engineering Aspects*, vol. 583, p. 123960, 2019.

[38] D. H. Choi, J. Lee, H. Hong, and Y. T. Kang, "Thermal conductivity and heat transfer performance enhancement of phase change materials (PCM) containing carbon additives for heat storage application," *International Journal of Refrigeration*, vol. 42, pp. 112–120, 2014.

[39] Y. A. Çengel and A. J. Ghajar, *Heat and mass transfer fundamentals & applications*. New York, NY: McGraw-Hill Education, 2015, pp. 539-544.

Appendix A

EES code that is used to find the properties of R134a, R600a, and R404a refrigerants, and to calculate the energetic and the exergetic coefficient of performance is presented in this appendix.

EES Code

R134a:

```
"Known information "

F$='r134a'

Q_dot_e=100 [J/s]          " cooling capacity"
T_2=40[C]                   "Superheated"  "Assumed "

T_1=1 [C]                    "evaporator temperature"

x_1=1                        "Saturated vapor"

T_3=35

x_3=0                        "Saturated liquid "  "Assumed "

eta_Comp=0.8          "Assumed "
"------------------------------------------------------------"

"STATE 1"

P_1=Pressure(F$,T=T_1,x=x_1)
h_1=Enthalpy(F$,T=T_1,x=x_1)
s_1=Entropy(F$,T=T_1,x=x_1)

"STATE 3"
P_3=Pressure(F$,T=T_3,x=x_3)

h_3=Enthalpy(F$,x=x_3,P=P_3)

rho_3l=Density(F$,x=0,P=P_3)
rho_3g=Density(F$,x=1,P=P_3)

cp_3l=Cp(F$,x=0,P=P_3)
cp_3g=Cp(F$,x=1,P=P_3)

h_3l=Enthalpy(F$,x=0,P=P_3)
h_3g=Enthalpy(F$,x=1,P=P_3)
```

```
mu_3l=Viscosity(F$,x=0,P=P_3)
mu_3g=Viscosity(F$,x=1,P=P_3)

DELTAh_vap=Enthalpy_vaporization(F$,P=P_3)
"STATE 4"
h_4=h_3
m_dot= Q_dot_e/(h_1- h_4)

"STATE 2"
P_2=P_3
h_2=Enthalpy(F$,T=T_2,P=P_2)
T_2_s=Temperature(F$,P=P_2,s=s_1)
h_2_s=Enthalpy(F$,P=P_2,s=s_1)
"------------------------------------------------------------"
 R= P_2/P_1                                   "pressure ratio"
"condenser"
Q_dot_c=m_dot * (h_2- h_3)

"compressor power"
W_in=m_dot * (h_2- h_1)/eta_Comp

"compressor  adiabatic efficiency"
e_comp=  (h_2_s- h_1)/(h_2- h_1)

"Coefficient of Performance"
COP=Q_dot_e / W_in

"Exergetic Coefficient of Performance"

COP_ex=COP*((T_3+273.15)-(T_1+273.15)) /(T_1+273.15)
```

Unit Settings: SI C kPa J mass deg

COP = 2.009	cp_{3g} = 1071 [J/kg-K]	cp_{3l} = 1450 [J/kg-K]
Δh_{vap} = 172373 [J/kg]	η_{Comp} = 0.8	e_{comp} = 0.304
F$ = 'R134a'	h_1 = 251613 [J/kg]	h_2 = 314115 [J/kg]
$h_{2,s}$ = 270612 [J/kg]	h_3 = 94645 [J/kg]	h_{3g} = 267017 [J/kg]
h_{3l} = 94645 [J/kg]	h_4 = 94645 [J/kg]	μ_{3g} = 0.00001223 [kg/m-s]
μ_{3l} = 0.000181 [kg/m-s]	$\dot{m}$ = 0.0006371 [kg/s]	P_1 = 314.8 [kPa]
P_2 = 787.1 [kPa]	P_3 = 787.1 [kPa]	$\dot{Q}_c$ = 139.8 [J/s]
$\dot{Q}_e$ = 100 [J/s]	R = 2.5	ρ_{3g} = 38.38 [kg/m^3]
ρ_{3l} = 1185 [kg/m^3]	s_1 = 930.3 [J/kg-K]	T_1 = 2 [C]
T_2 = 77 [C]	$T_{2,s}$ = 34.12 [C]	T_3 = 30.74 [C]
W_{in} = 49.77 [J/s]	x_1 = 1	x_3 = 0

Figure A.1: R134a

R600a

"Known information "

F$=' R600a'

Q_dot_e=100 [J/s] " cooling capacity"
T_2=40[C] "Superheated" "Assumed "

T_1=1 [C] "evaporator temperature"

x_1=1 "Saturated vapor"

T_3=35

x_3=0 "Saturated liquid " "Assumed "

eta_Comp=0.8 "Assumed "
"--"

"STATE 1"

P_1=Pressure(F$,T=T_1,x=x_1)
h_1=Enthalpy(F$,T=T_1,x=x_1)
s_1=Entropy(F$,T=T_1,x=x_1)

"STATE 3"

P_3=Pressure(F$,T=T_3,x=x_3)

h_3=Enthalpy(F$,x=x_3,P=P_3)

rho_3l=Density(F$,x=0,P=P_3)
rho_3g=Density(F$,x=1,P=P_3)

cp_3l=Cp(F$,x=0,P=P_3)
cp_3g=Cp(F$,x=1,P=P_3)

h_3l=Enthalpy(F$,x=0,P=P_3)
h_3g=Enthalpy(F$,x=1,P=P_3)

mu_3l=Viscosity(F$,x=0,P=P_3)
mu_3g=Viscosity(F$,x=1,P=P_3)

DELTAh_vap=Enthalpy_vaporization(F$,P=P_3)

"STATE 4"

```
h_4=h_3
m_dot= Q_dot_e/(h_1- h_4)

"STATE 2"
P_2=P_3

h_2=Enthalpy(F$,T=T_2,P=P_2)
T_2_s=Temperature(F$,P=P_2,s=s_1)
h_2_s=Enthalpy(F$,P=P_2,s=s_1)
"------------------------------------------------------------"
 R= P_2/P_1                                  "pressure ratio"

"condenser"
Q_dot_c=m_dot * (h_2- h_3)

"compressor power"
W_in=m_dot * (h_2- h_1)/eta_Comp

"compressor  adiabatic efficiency"
e_comp=  (h_2_s- h_1)/(h_2- h_1)

"Coefficient of Performance"
COP=Q_dot_e / W_in

"Exergetic Coefficient of Performance"

COP_ex=COP*((T_3+273.15)-(T_1+273.15)) /(T_1+273.15)
```

Unit Settings: SI C kPa J mass deg

$COP = 1.725$	$cp_{3g} = 1885$ [J/kg-K]	$cp_{3l} = 2553$ [J/kg-K]
$\Delta h_{vap} = 314076$ [J/kg]	$\eta_{Comp} = 0.8$	$e_{comp} = 0.2689$
F$ = 'r600a'	$h_1 = 679992$ [J/kg]	$h_2 = 807380$ [J/kg]
$h_{2,s} = 714247$ [J/kg]	$h_3 = 405294$ [J/kg]	$h_{3g} = 719370$ [J/kg]
$h_{3l} = 405294$ [J/kg]	$h_4 = 405294$ [J/kg]	$\mu_{3g} = 0.00000818$ [kg/m-s]
$\mu_{3l} = 0.0001492$ [kg/m-s]	$\dot{m} = 0.000364$ [kg/s]	$P_1 = 169.2$ [kPa]
$P_2 = 422.9$ [kPa]	$P_3 = 422.9$ [kPa]	$\dot{Q}_c = 146.4$ [J/s]
$\dot{Q}_e = 100$ [J/s]	$R = 2.5$	$\rho_{3g} = 11.05$ [kg/m^3]
$\rho_{3l} = 542.4$ [kg/m^3]	$s_1 = 3746$ [J/kg-K]	$T_1 = 2$ [C]
$T_2 = 77$ [C]	$T_{2,s} = 31.64$ [C]	$T_3 = 31.64$ [C]
$W_{in} = 57.97$ [J/s]	$x_1 = 1$	$x_3 = 0$

Figure A.2: R600a

R404a

"Known information "

F$=' R600a'

Q_dot_e=100 [J/s] " cooling capacity"
T_2=40[C] "Superheated" "Assumed "

T_1=1 [C] "evaporator temperature"

x_1=1 "Saturated vapor"

T_3=35

x_3=0 "Saturated liquid " "Assumed "

eta_Comp=0.8 "Assumed "
"--"

"STATE 1"

P_1=Pressure(F$,T=T_1,x=x_1)
h_1=Enthalpy(F$,T=T_1,x=x_1)
s_1=Entropy(F$,T=T_1,x=x_1)

"STATE 3"

P_3=Pressure(F$,T=T_3,x=x_3)

h_3=Enthalpy(F$,x=x_3,P=P_3)

rho_3l=Density(F$,x=0,P=P_3)
rho_3g=Density(F$,x=1,P=P_3)

cp_3l=Cp(F$,x=0,P=P_3)
cp_3g=Cp(F$,x=1,P=P_3)

h_3l=Enthalpy(F$,x=0,P=P_3)
h_3g=Enthalpy(F$,x=1,P=P_3)

mu_3l=Viscosity(F$,x=0,P=P_3)
mu_3g=Viscosity(F$,x=1,P=P_3)

DELTAh_vap=Enthalpy_vaporization(F$,P=P_3)

"STATE 4"
h_4=h_3

m_dot= Q_dot_e/(h_1- h_4)

"STATE 2"
P_2=P_3

h_2=Enthalpy(F$,T=T_2,P=P_2)
T_2_s=Temperature(F$,P=P_2,s=s_1)
h_2_s=Enthalpy(F$,P=P_2,s=s_1)
"--"
R= P_2/P_1 "pressure ratio"

"condenser"
Q_dot_c=m_dot * (h_2- h_3)

"compressor power"
W_in=m_dot * (h_2- h_1)/eta_Comp

"compressor adiabatic efficiency"
e_comp= (h_2_s- h_1)/(h_2- h_1)

"Coefficient of Performance"
COP=Q_dot_e / W_in

"Exergetic Coefficient of Performance"

COP_ex=COP*((T_3+273.15)-(T_1+273.15)) /(T_1+273.15)

Unit Settings: SI C kPa J mass deg

$COP = 1.478$	$cp_{3g} = 1380$ [J/kg-K]	$cp_{3l} = 1657$ [J/kg-K]	$\Delta h_{vap} = 128596$ [J/kg]
$\eta_{Comp} = 0.8$	$e_{comp} = 0.2857$	F$ = 'R404a'	$h_1 = 366782$ [J/kg]
$h_2 = 429540$ [J/kg]	$h_{2,s} = 384713$ [J/kg]	$h_3 = 250849$ [J/kg]	$h_{3g} = 379445$ [J/kg]
$h_{3l} = 250849$ [J/kg]	$h_4 = 250849$ [J/kg]	$\mu_{3g} = 0.0000139$ [kg/m-s]	$\mu_{3l} = 0.0001106$ [kg/m-s]
$\dot{m} = 0.0008626$ [kg/s]	$P_1 = 639.5$ [kPa]	$P_2 = 1599$ [kPa]	$P_3 = 1599$ [kPa]
$\dot{Q}_c = 154.1$ [J/s]	$\dot{Q}_e = 100$ [J/s]	$R = 2.5$	$\rho_{3g} = 87.09$ [kg/m^3]
$\rho_{3l} = 996.1$ [kg/m^3]	$s_1 = 1607$ [J/kg-K]	$T_1 = 2$ [C]	$T_2 = 77$ [C]
$T_{2,s} = 38.78$ [C]	$T_3 = 34.47$ [C]	$W_{in} = 67.67$ [J/s]	$x_1 = 1$
$x_3 = 0$			

Figure A.3: R4040a

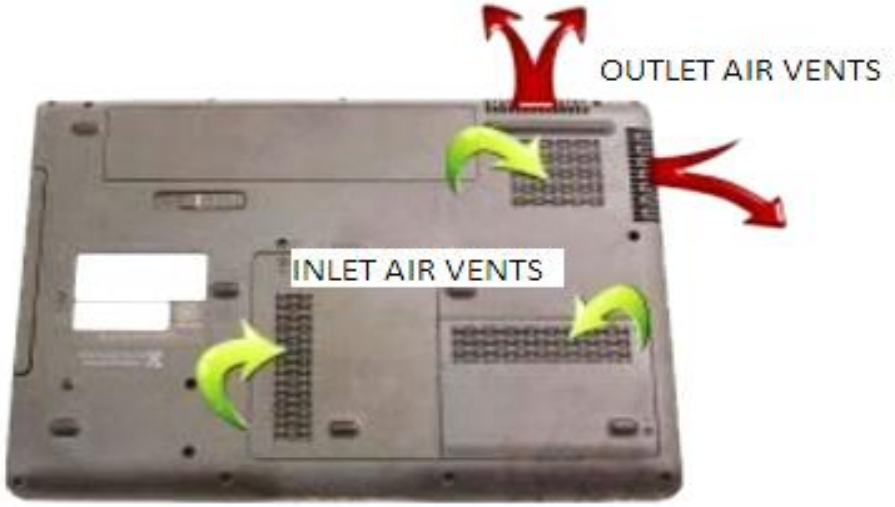

Figure A.4: bottom view of laptop

ANSYS Simulation Results

Graphs for temperature contour of the heat sink at various times are presented in Figures A.5- A.10.

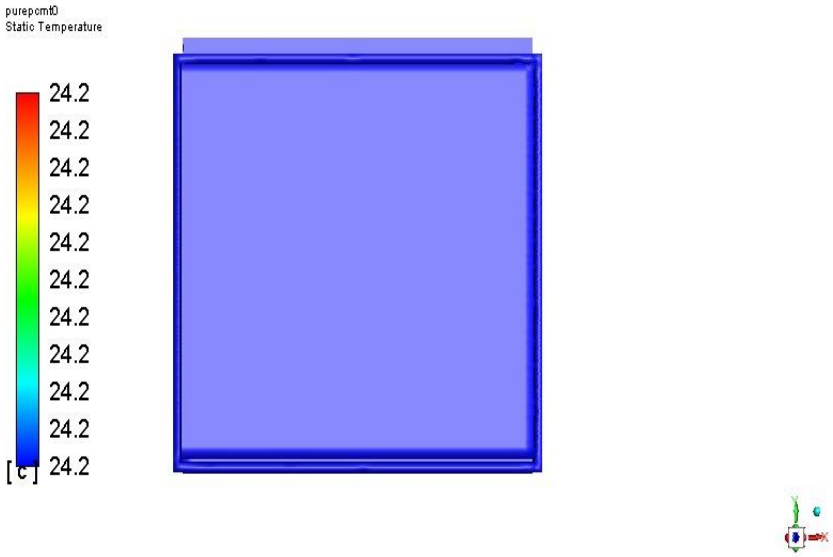

Figure A.5: bottom view of laptop

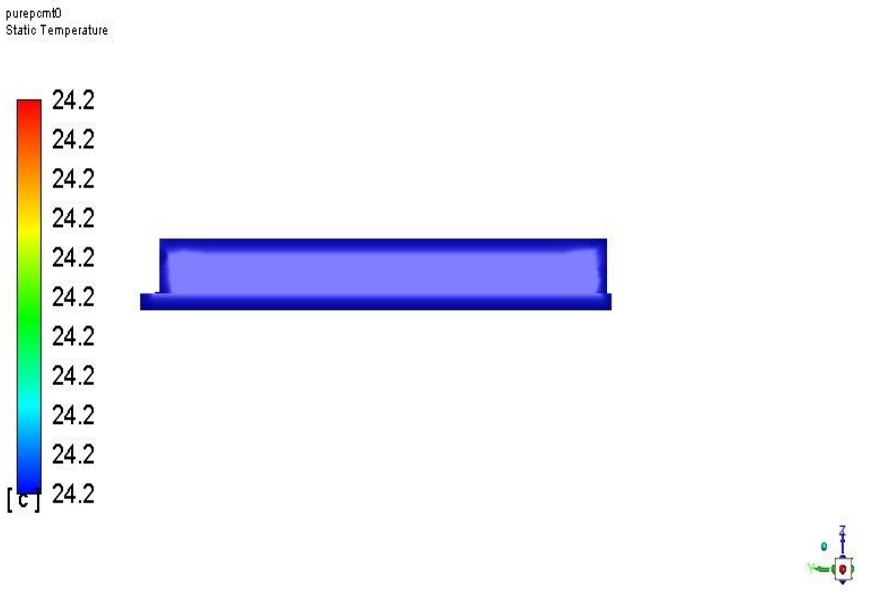

Figure A.6: Temperature contour of the heat sink at t=0s (side view).

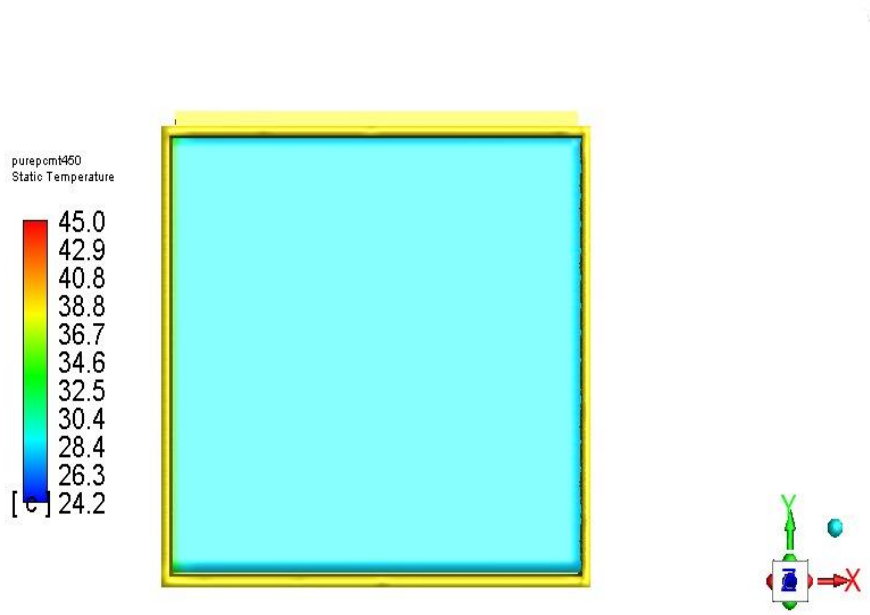

Figure A.7: Temperature contour of the heat sink at t=450s (top view).

Figure A.8: Temperature contour of the heat sink at t=450s (side view).

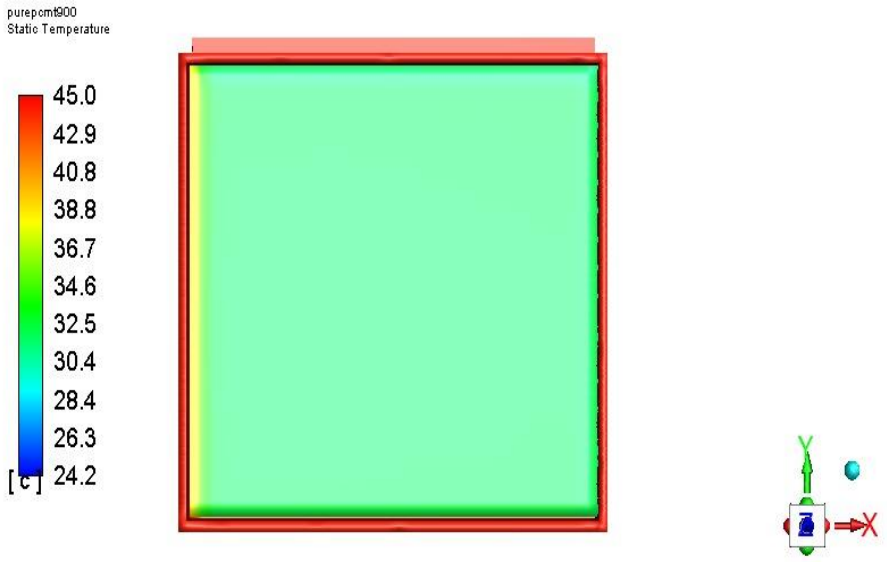

Figure A.9: Temperature contour of the heat sink at t=900s (top view).

Figure A.10: Temperature contour of the heat sink at t=9000s (side view).

Vita

Yahya Sheikh was born in 1993, in United Arab Emirates. He received his primary and secondary education in Abu Dhabi, UAE. He received his B.Sc. degree in Mechanical Engineering from University of Sharjah in 2017.

In February 2018, he joined the Mechanical Engineering master's program in the American University of Sharjah as a graduate teaching assistant. His research interests are in PCM, Thermal management and renewable energy.